NASA/CR- 97- 207499

IN-27-CR
076892

Final Report for
Cooperative Agreement NCC3-225
NASA-Lewis Research Center
by The University of Akron

"Organometallic Polymeric Conductors"

Chemistry Department
The University of Akron
Akron, Ohio

UA Technical Director: Dr. Wiley J. Youngs, P. I. (330) 972-5362

LeRC Technical Director: Dr. Mary Ann Meador (216) 433-3221

UA Business Contact: Gerald Parker, Director of Research Services and Sponsored Programs, The University of Akron, Akron, Ohio 44325-2102, Tel. (330) 972-7666

Table of Contents

Final Report for Cooperative Agreement NCC3-225:

Optimization Study of Electrically Conductive Polymers

For aerospace applications, the use of polymers can result in tremendous weight savings over metals.[1] Suitable polymeric materials for some applications like EMI shielding, spacecraft grounding, and charge dissipation must combine high electrical conductivity with long-term environmental stability, good processability, and good mechanical properties. Recently, other investigators have reported hybrid films made from an electrically conductive polymer combined with insulating polymers[2]. In all of these instances, the films were prepared by infiltrating an insulating polymer with a precursor for a conductive polymer (either polypyrrole or polythiophene), and oxidatively polymerizing the precursor *in situ*. The resulting composite films have good electrical conductivity, while overcoming the brittleness inherent in most conductive polymers.

The highest conductivities reported (approximately 4 Scm^{-1}) were achieved with polythiophene in a polystyrene host polymer[2h]. The best films using a polyamide as base polymer[2e,f] were four orders of magnitude less conductive than the polystyrene films. The authors suggested that this was because polyimides were unable to swell sufficiently for infiltration of monomer as in the polystyrene. It was not clear, however, if the different conductivities obtained were merely the result of differing oxidation conditions. Oxidation time, temperature and oxidant concentration varied widely among the studies.

Many aerospace applications require a *combination* of properties. Thus, hybrid films made from polyimides or other engineering resins are of primary interest, but only if conductivities on the same order as those obtained with a polystyrene base could be obtained. Hence, a series of experiments was performed to optimize the conductivity of polyimide-based composite films. The polyimide base chosen for this study was Kapton®. 3-Methylthiophene (3MT) was used for the conductive phase.

Three processing variables were identified for producing these composite films, namely time, temperature, and oxidant concentration for the *in situ* oxidation. Statistically designed experiments were used to examine the effects of these variables and synergistic/interactive effects among variables on the electrical conductivity and mechanical strength of the films.

Temperatures were varied from -10 to 30 C, times from 2 to 8 hours and oxidant concentrations from 0.4 to 1.2 M. The experiments were carried out in a randomized order. Kapton films were soaked for 24 hours at room temperature with stirring in 3MT. The monomer-treated films were then oxidized under the selected design conditions. Conductivity of all the films was measured with a standard four-point test using DC current. Maximum

mechanical stress at maximum load was also measured for all the films with a tensile test. The measured values obtained under different oxidation conditions for each of the films were analyzed by multiple linear regression. The conductivities were log transformed before analysis.

Multiple linear regression of log conductivity gave a six-term model. Reaction time, temperature, and oxidant concentration were all found to have a significant linear effect on the log conductivity, and all three variables interacted strongly with each other. The predicted conductivity response surface for p-3MT/Kapton with oxidant concentration held constant at 1.2 M is shown. The maximum achievable conductivity within the design space was predicted to be 5.7 Scm^{-1} by oxidizing for 8 hours at 30 in 1.2 M $FeCl_3$. For three different experimental runs under these optimum conditions, the mean value was 4.97 Scm^{-1}. This is in good agreement with the predicted optimum and as high as previously reported with polystyrene as the base polymer.

Multiple linear regression analysis of the tensile data revealed that temperature and time have the greatest effect on maximum stress. The response surface of maximum stress *vs.* temperature and time (for oxidant concentration at 1.2 M) is shown. At the oxidation conditions predicted to give maximum conductivity for p-3MT/Kapton, the maximum stress is predicted to be 27000 PSI. If better mechanical properties are needed, compromise conditions can be chosen from the response surface models that give slightly lower conductivities. For example, to obtain predicted maximum stress values closer to untreated Kapton (around 34000 PSI) for p-3MT/Kapton, oxidation time can be limited to two hours or temperature can be lowered to 10 C. For a two hour oxidation, the optimal conditions of 30 C and 1.2 M $FeCl_3$ still yield a predicted conductivity in excess of 1.5 Scm^{-1}.

Conductivity of the composite films was measured for over 150 days in air at ambient temperature. The conductivity of the films dropped only half an order of magnitude in that time. Films aged under vacuum at ambient temperature diminished slightly in conductivity in the first day, but did not change thereafter. This suggests that if the films are protected from air and perhaps moisture, the conductivity will persist indefinitely.

The successful in-situ polymerization of Kapton films with 3-methylthiophene suggests that this technique may be suitable for other polymer substrates. Experimental efforts will examine the effects of this experimental scheme on the electrical conductivity of PMC's (Polymer Matrix Composites). Some of the PMC components that would benefit from an electrically conductive surface possess irregular geometries. If successful the surface treatment of these structures to form an environmentally stable, structurally continuous,

electrically conductive layer may broaden the application for electrically conductive polymer matrices.

The PMC's of interest are two-phase systems. One phase consists of a structural support material which provides the mechanical integrity of the composite. Two examples of supports used in fabrication include woven fiberglass mats and carbon fibers . The neat resin phase used in PMC's serves as a composite filler. The resin is used as a viscous solution to fill vacant regions in the support cloth and varies in functionality from low-temperature utilization epoxies to high temperature polyimides. The two materials are subjected to a cure cycle of heating with or without applied pressure in a mold.

A PMC-conductive polymer alloy must overcome complications not encountered in the Kapton-conductive polymer composite. The comparitively single-phased Kapton is replaced by a host structure with the potential for additional adverse chemical interactions. Resin processability and morphology are only two factors that play a role in the integrity of the resultant polymer matrix. Consequently the investigation of neat resin chemistry is an integral factor in the experimental investigation. The effect of the neat resin on the mechanical properties, thermo-oxidative stability, and performance are issues that must be addressed. An experimental design approach will be applied to maximize the efficiency of the laboratory effort. The material properties (initial and long term) will also be monitored and assessed. The experimental results will add to the existing database for electrically conductive polymer materials.

Polymerization of Disubstituted Diacetylenes

The topochemical 1,4-addition polymerization of disubstituted diacetylenes in the solid state to form polydiacetylenes (PDAs) has been studied extensively since its discovery in the late 1960's.[3] The reaction can be initiated by ultra violet radiation, gamma radiation, thermal heating or mechanical stress. The propagating species is believed to be a triplet carbene initiated thermally, photochemically with ultraviolet or γ-ray radiation, or by mechanical stress. [4,5] The resulting polymer often has a metallic luster and is not as soluble as the monomer. This solubility difference can be used to determine the degree of polymerization. Polydiacetylenes have extensive p-conjugation along the backbone. This conjugation allows the polymers to have good conducting properties when doped, and good third order non-linear optical properties. Possible applications are as photonic[6] or electronic[7,8] devices.

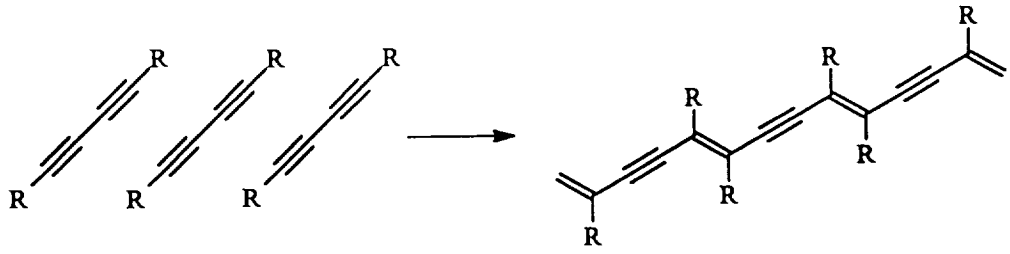

Figure 1. Example of a 1,4 addition polymerization of a diacetylene.

Delocalizing substituents, such as an aromatic ring, bound directly to the diacetylene have been predicted to maximize conductivity and nonlinear optical properties.[9,10] However, monomers with an aromatic moiety bound directly to the diacetylenic linkage as in diphenylacetylene and dicarbazolyl diacetylene do not readily polymerize.[11] Studies have shown that the orientation of monomers in the crystal lattice are important for polymerization to occur. It has been suggested that diactylenes with aromatic substituents tend to stack with the aromatic rings over top of each other, so that the atoms that would be involved in the 1,4-addition polymerization are to far apart to interact. Monomers found to polymerize usually pack at a distance of 4.4-5.4Å and have an angle of incidence of 39-58§ between the diacetylene units in two molecules.[12] Two other monomers with an aromatic substituent bound to the diacetylene moiety have recently appeared in the literature.[13,14]

We have synthesized a cyclic diacetylene in which the monomer has two aromatic substituents bound directly to the diacetylene moiety. Iodination of phenylacetylene[15] followed by silylation of the *o*-iodophenylacetylide anion with trimethylsilylchloride produced **1**. *o*-Diethynylbenzene[16] was combined with two equivalents of **1** in the presence of a palladium-copper catalyst and the product **2** desilylated to yield **3**. The intramolecular Hay[17] coupling of **3** gave the cyclynediyne **4**.

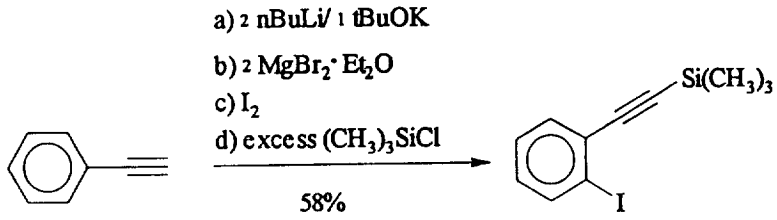

1

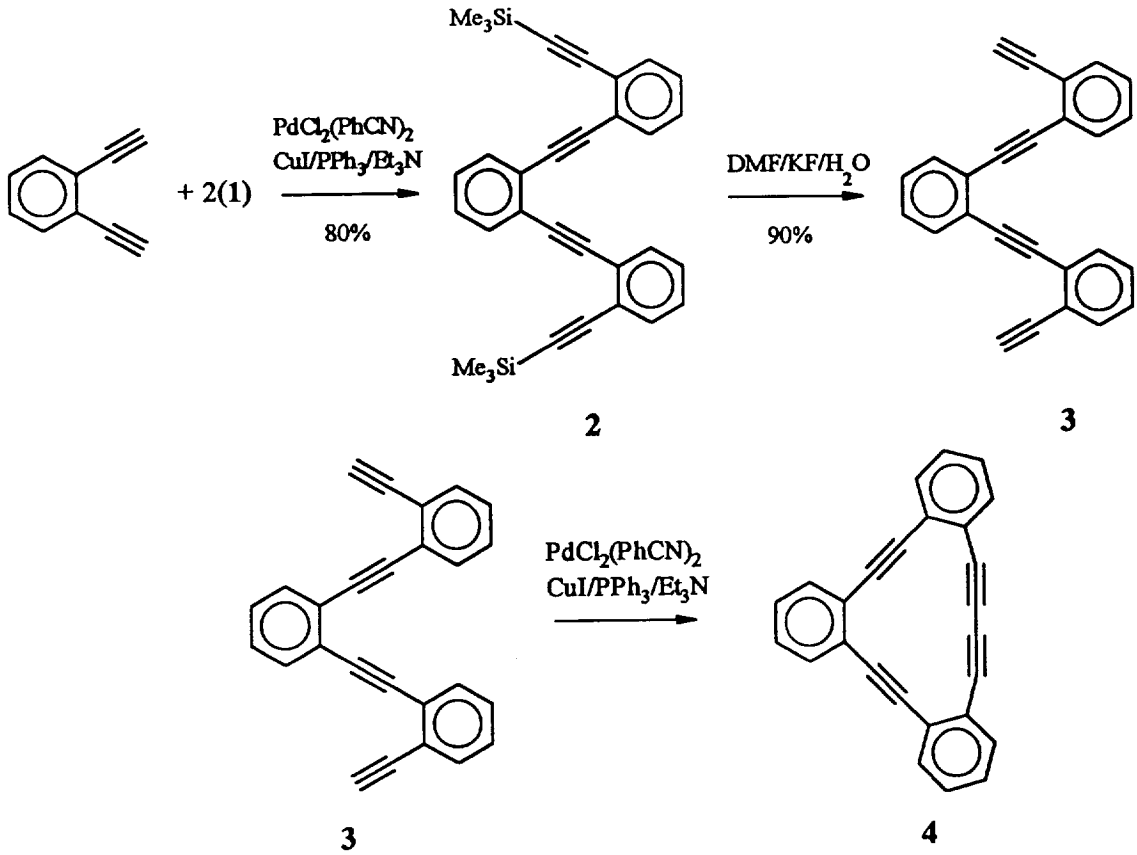

Recrystallizing compound **4** by slow evaporation from ethyl acetate in hexanes in the absence of light resulted in the formation of yellow needle-like crystals. Solution of the the X-ray structure[18] showed that the packing the diacetylene linkage in the monomer is bent (see Figure 2) and the packing parameters are slightly out of the range expected for polymerizable monomers. The distance between diacetylenes in two molecules is 6.323Å and the angle of incidence is 34.4° (see Figure 3). However, exposing the yellow crystals to light results in the formation of a violet layer on the surface having a metallic luster. Washing with acetone yields a yellow solution with an insoluble violet solid on the bottom. Evaporating the acetone results in the recovery of compound **4**. The polymerizability may be aided by the presence of strain along the bent diacetylene linkage. This strain may make it possible for the monomer to polymerize even though the packing parameters are outside the normal observed range for polymerizable monomers.

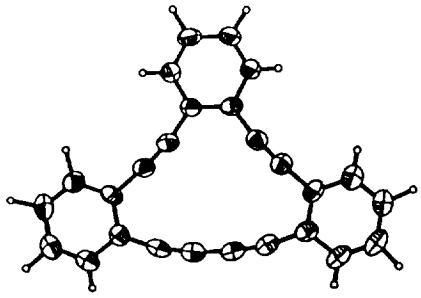

Figure 2: Ortep of Compound 4 drawn at 50% probability.

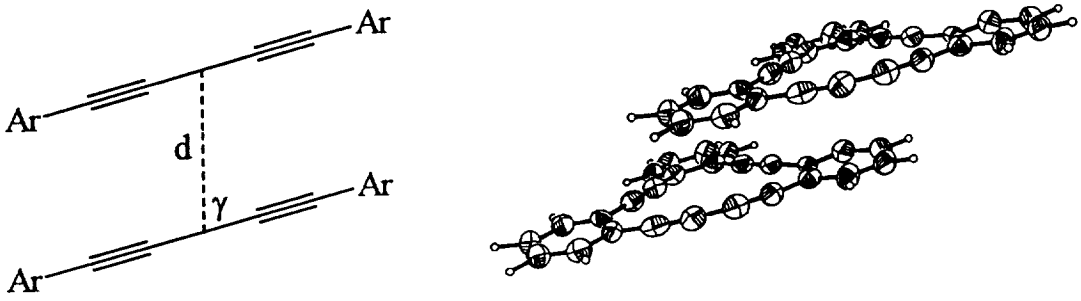

Figure 3. Packing parameters shown of compound 4 (d = 6.323Å, γ = 34.4°).

Further analysis was accomplished with TGA, DSC and ^{13}C solid state NMR. DSC exhibited an exothermic peak at 145°C in nitrogen and at 155 C in air. TGA of compound 4 showed no appreciable weight loss at this temperature in nitrogen. TGA in air indicated an initial loss of weight at the exotherm and then a gain of weight with further heating. The gain of weight may be explained as oxygen quenching the propagating radicals. A comparison was done between the solid state ^{13}C NMR of compound 4 and that of the violet solid that remained from the acetone wash. In addition to slight chemical shifts, two new peaks at 149.98 and 145.07 were observed in the violet solid that were not present with compound 4. The alkynyl region broadened, and relative peak heights changed, but it did not completely dissappear which is evident that a graphitic substance was not produced.

Compound 4 was heated at 145-150°C for a period of 24 hours in the dark with an argon gas purge. A violet solid with a film-like consistency resulted. DSC exhibited no exotherm at 145°C and no weight loss was observed with TGA until 400°C. It was insoluble in acetone, but was slightly soluble in chlorinated polar solvents. Compound 4 also appears to

polymerize under mechanical stress. Pressing the yellow solid for one hour at 20000 psi yielded a violet plate.

Further discussions of this chemistry are presented in the attached papers.

Publications resulting from support by the NASA-Lewis Research Facility

1. Kathy C. Chuang, James D. Kinder, Diana L. Hull, Wiley J. Youngs "Rodlike Polyimides", *Polym. Prepr.*, **1994**, *35*, 341-2.
2. Kyle P. Baldwin, Claire A. Tessier, Wiley J. Youngs, "Solid State Polymerization of a Strained Cyclic Diacetylene" *Polym. Prepr.* **1994**, *35*, 546.
3. Kyle P. Baldwin, Adam J. Matzger, Daniel Scheiman, Claire A. Tessier, K. Peter C. Vollhardt, Wiley J. Youngs, "Synthesis, Crystal Structure, and Polymerization of 1,2:5,6:9,10-Trbenzo-3,7,11,13-tetrdehydr[14} annulene", *Synlett*, **1995**, 1215-1218.
4. Aryeh A. Frimer, James D. Kinder, Wiley J. Youngs, Mary Ann B. Meador, "Reinvestigation of the Photocylcization of 1,4-Phenylene Bis(phenylmaleic anhydride): Preparation and Structure of [5]Helicene 5,6:9,10-Dianhydride", *J. Org. Chem.* **1995**, *60*, 1658-1664.
5. Kyle P. Baldwin, Claire A. Tessier, Wiley J. Youngs, "Cyclic Ortho Substituted Benzo-Alkynes," in *The Polymeric Materials Encyclopedia*, J. C. Salamone, Ed., CRC Press: Baca Raton, FL, 1996.
6. Kathy C. Chuang, James D. Kinder, Diana L. Hull, David B. McConville, Wiley J. Youngs, "Rigid-Rod Polyimides Based on Noncoplanar 4,4'-Biphenyldiamines: A Review of Polymer Properties vs Configuration of Diamines", *Macromolecules*, **1997**, *30*, 7183-7190.
7. Kyle P. Baldwin[a], Rick Simons[a], Dan Scheiman[b], Robert Lattimer[c], Claire A. Tessier[a], Wiley J. Youngs[a,*], "Synthesis, Characterization and Crystal Structures of Two Strained Cyclic Diacetylenes and Their Precursors", *J. Chem. Cryst.* Accepted for publication.

---

[1] Meador, M.A.B.; Gaier, J.R.; Good, B.S.; Sharp, G.R.; Meador, M.A. *Sampe Quarterly*, **1990**, 23,.

[2] a. Li, C.; Song, Z.; *Synth. Metals*, **1991**, *40*, 23.
b. Stanke, D.; Hallensleben, M.L.; Toppare, L.; *Synth. Metals*, **1993**, *55-57*, 1108.
c. Morita, M.; Hashida, I.; Nishimura, M.; *J. Appl. Polym. Sci.*, **1988**, *36*, 1639.
d. Van Duk, H.; Aagaard, O.; Schellekens, R.; *Synth. Metals*, **1993**, *55-57*, 1085.
e. Tieke, B.; Gabriel, W.; *Polymer*, **1990**, *31*, 20.
f. Dao, L.H.; Zhong, X.F.; Menikh, A.; Paynter, R.; Martim, F.; *Annu. Tech. Conf.-Soc.*, Plast., Eng., **1991**, *49*, 783.
g. Ruckenstein, E.; Park, J.S.; *Polymer Composites*, **1991**, *12(4)*, 289.
h. Ruckenstein, E.; Park, J.S.; *Synth. Metals*, **1991**, *44*, 293-306.

[3] Wegner, G. *Z. Naturforsch.* **1969**, *24b*, 824.

[4] Chance, R.R.; Patel, G.N. *J. Polym. Sci. Polym. Phys. Ed.*, **1978**, *16*, 859.

[5] Baughman, R.H. *J. Polym. Sci. Polym. Phys. Ed.*, **1974**, *12*, 1511.

[6] Sauteret, C.; Herman, J.P.; Frey, R.; Pradere, F.; Ducuing, J.; Baughman, R.H., Chance, R.R. *Phys. Rev. Lett.*, **1976**, *36(16)*, 956.

[7] Bredas, J.L.; Chance, R.R.; Baughman, R.H.; Silbey, R. *J. Chem. Phys.*, **1982**, *76(7)*, 3673.
[8] Nakanishi, H.; Matsuda, H.; Kato, M. *Mol. Cryst. Liq. Cryst.*,**1984**, *105*, 77.
[9] Matsuda, H; Nakanishi, H; Kato, S; Kato, M. *J. Polym. Sci., Pol. Chem. Ed.*, **1987**, *25*, 1663.
[10] Orchard, B.J.; Tripathy, S.K. *Macromolecules*, **1986**, *19*, **1844**.
[11] Mayerle, J.J.; Flandera, M.A. *Acta Cryst.*, **1978**, *B34*, 1374.
[12] Baughman, R.; Chance, R.R. *Ann. N.Y. Acad. Sci.*, **1978**, *313*, 705.
[13] Kim, W.H.; Kodali, N.B.; Kumar, J.; Tripathy, S.K. *Macromolecules*, **1994**, *27*, 1819.
[14] Zhou, Q.; Carroll, P.J.; Swager, T.M. *J. Org. Chem.*, **1994**, *59*, 1294.
[15] Hommes, H.; Verkruijsse, H.D.; Brandsma, L. *Tetrahedron Lett.* **1981**, *22*, 2495.
[16] Huynh, C.; Linstrumelle, G. *Tetrahedron*, **1988**, *44*, 6337.
[17] Hay, A.S. *J. Org. Chem.*, **1962**, *27*, 3320.
[18] Crystal data for $C_{26}H_{12}$, monoclinic, $P2_1/c$, a = 16.339 (3), b = 6.323 (1), c = 17.043 (2) Å. β = 100.22 (1)°, Z = 4, V = 1732.8 (5) Å^3, D_c = 1.243 g/cm^3, Mo-K_α radiation, λ = 0.71073 Å, $3.5 \leq 2\theta \leq 45°$. Syntex $P2_1$ diffractometer. 2265 reflections were collected of which 1332 unique reflections [$F > 4.0\ \sigma(F)$] were used for refinement (235 parameters), converging to R = 0.0570 and R_w = 0.1109.

Synthesis, Crystal Structure, and Polymerization of 1,2:5,6:9,10-Tribenzo-3,7,11,13-tetradehydro[14]annulene

Kyle P. Baldwin[a], Adam J. Matzger[b], Daniel A. Scheiman[c], Claire A. Tessier[a], K. Peter C. Vollhardt[b]*, Wiley J. Youngs[a]*

[a]Department of Chemistry, University of Akron, Akron, Ohio 44325-3601, USA
Fax 216 972 7370; youngs@atlas.chemistry.uakron.edu
[b]Department of Chemistry, University of California-Berkeley and the Chemical Sciences Division, Lawrence Berkeley Laboratory, Berkeley, CA 94720-1460, USA
Fax 510 643 5208; vollhard@cchem.berkeley.edu
[c]Nyma Inc., 21000 Brookpark Road, Cleveland, Ohio 44135, USA
Received 8 September 1995

Abstract: The title compound constitutes a strained [14]annulene incorporating a 1,3-diyne unit amenable to topochemical polymerization.

Poly-1,3-diynes have attracted considerable attention since their solid state topochemical synthesis in 1969 by Wegner.[1] Possible applications are as photonic[1,2] and electronic devices.[1,3] In order for topochemical polymerization to occur most efficiently, the diyne monomers should pack in an offset manner at a stacking distance $d \sim 5$Å and an angle between the molecular and stacking axis $\gamma \sim 45°$ (Figure 1), although these figures appear to be only suggestive and

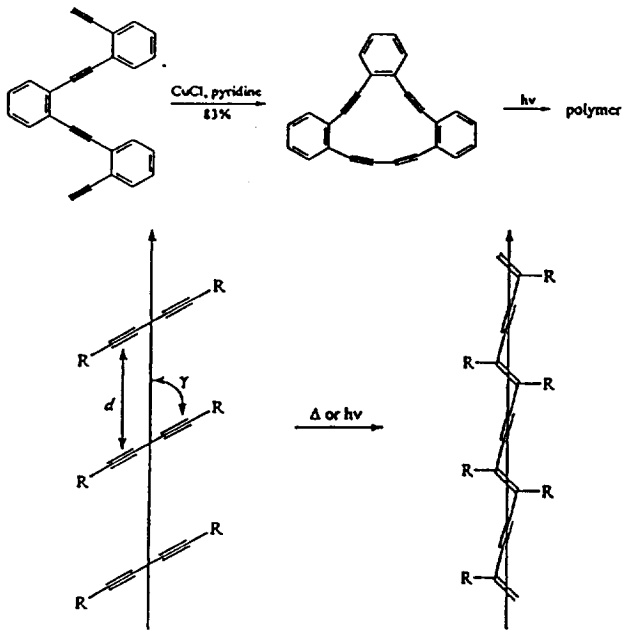

Figure 1. Topochemical diyne polymerization.

not exclusive.[1c,d,e,h] The propagating species are believed to have radicaloid-carbenoid character[1g,4] and can be generated thermally, by irradiation, or mechanical stress. The resulting polymer is usually highly colored, with a metallic luster, and often insoluble. Conjugating substituents, such as aryl, might improve conducting and optical properties, and this notion has been successfully tested with some derivatives,[1,5] but not with others, such as the parent diphenyldiacetylene.[5a,6] The solid state reactivity of cyclic analogs is relatively unexplored,[1d,1,7] especially that of all-carbon based, strained conjugated π-systems (dehydrobenzoannulenes).[8] The latter are of interest as they may give rise to polyenynes fused to a conjugated backbone. We report here the synthesis and polymerization of the tribenzodehydro[14]annulene 2, a cyclically delocalized, strained "diphenyldiyne monomer."

The colorless, very light-sensitive title compound 2 was obtained in remarkable yield by the intramolecular oxidative coupling of tetrayne 1[9] with cuprous chloride in pyridine-methanol, followed by chromatography on silica (acetone-hexanes, 5:95) (Scheme 1).[10] The

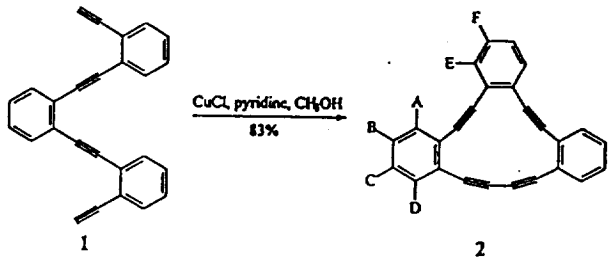

Scheme 1

spectral data are in accord with the assigned structure.[11] The field desorption mass spectrum as well as the low energy laser desorption time of flight (*vide infra*) measurement, showed a clean molecular ion for monomer 2. On electron impact mass analysis, loss of H_{1-4} and, in addition, C_2H_{1-6} occurred and a set of peaks for doubly charged ions is evident.[12] The ^{13}C NMR spectrum revealed the expected 13 lines and 1,3-diynyl carbon chemical shifts slightly deshielded relative to a number of appropriate model compounds,[8a,b,9,13] indicative of the presence of some strain in the molecule.[14] A quantitative measure of the latter is given by comparing the heats of the reactions - 2 RC≡CH → RC≡CC≡CR + H_2 - for phenylacetylene and 1: $\Delta\Delta H° \sim +9.4$ kcal mol^{-1} (MNDO-PM3). The ^1H NMR spectrum was analyzed completely by 2D NMR[15] and spectral simulation. Its most noticeable feature is the relatively low field chemical shifts, especially of $H_{A,D,E}$, in comparison with the corresponding absorptions of acyclic, non-, or anti-aromatic models (including 1),[8a,b,9,13,16] signaling diatropicity and therefore aromatic delocalization, at least by the NMR criterion.[17,18,19] The electronic spectrum exhibits a longest wavelength band at 365 nm, shifted bathochromically from that of 1 by 50 nm, and similar to that of other benzodehydro[14]annulenes.[13] The IR spectrum shows diynyl bands at 2216 and 2130 cm^{-1}, as well as a strong aromatic signal at 755 cm^{-1}.

Because of the novelty of the compound and in order to probe its suitability as a monomer to topochemical polymerization an x-ray structural investigation was undertaken. Slow evaporation of an ethyl acetate-hexanes (5:95) solution of 2 in the absence of light resulted in the formation of needle-like crystals. X-ray data were collected on a $P2_1$ diffractometer using molybdenum radiation.[20] The structure was successfully solved using direct methods and refined with SHELXL93 (Figure 2).[21] Even cursory visual inspection indicates that the molecule is significantly distorted, the monoyne units bending inwards (3.9-11.5°), whereas the diynyl moiety is deflected to the outside (8.6-11.2°) of the annulene ring. Significantly, the packing pattern (Figure 3) juxtaposes the diyne fragments in the prerequisite way for polymerization,[1] although the packing parameters are on the fringe of

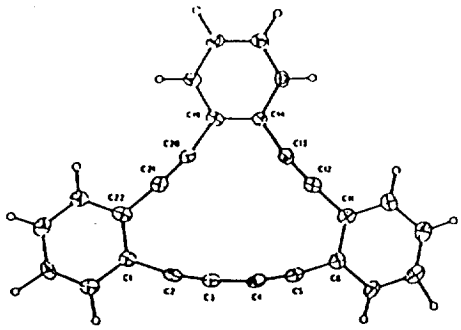

Figure 2. Thermal ellipsoid plot of compound 2 drawn at 50% probability. Selected bond lengths (Å) and angles (°): C1-C2 1.43, C2-C3 1.20, C3-C4 1.36, C4-C5 1.22, C5-C6 1.42, C11-C12 1.44, C12-C13 1.21, C13-C14 1.43, C-C_{arom}(avg) 1.393 (range 1.37-1.41); C1-C2-C3 168.8, C2-C3-C4 171.4, C3-C4-C5 170.9, C4-C5-C6 171.0, C5-C6-C11 118.9, C6-C11-C12 120.9, C11-C12-C13 176.1, C12-C13-C14 169.3, C13-C14-C19 124.5, C14-C19-C20 124.6, C19-C20-C21 168.5, C20-C21-C22 175.2, C21-C22-C1 122.7, C22-C1-C2 117.2, C-C-C_{arom}(avg) 120.0 (range 118.7-121.5).

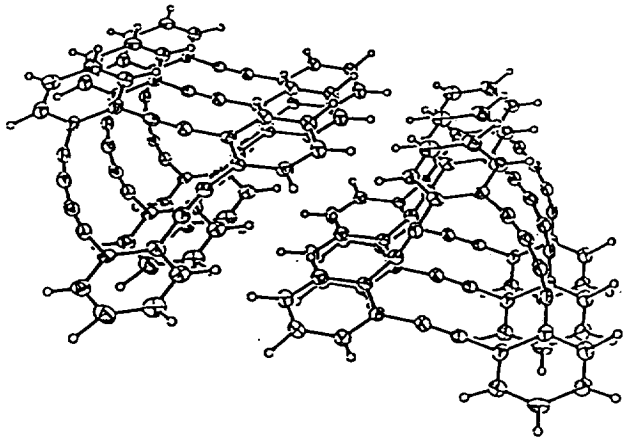

Figure 3. Packing of compound 2 (d = 6.308 Å, γ = 35.5°, S_1 = 3.66).

the observed range for such monomers. Nevertheless, exposure of crystals of 2 to light rapidly generated a violet surface layer exhibiting a metallic luster. Prolonged irradiation did not significantly increase the degree of conversion, presumably because the bulk material became impenetrable to the incident light.[1] Extraction with acetone removed intact 2 and left an insoluble violet solid. A similar, but complete transformation could be effected by applying pressure (20,000 psi, 1 h) to a crystal of 2, turning it into a insoluble violet plate. That polymerization is occurring could be nicely demonstrated by high energy laser desorption time of flight mass spectrometry of 2 allowing the detection of oligomers containing up to 9 units (Figure 4). To our knowledge this constitutes the first application of the technique to topochemical polymerizations of molecules of the type 2.[22] Instructive is also a comparison of the solid state ^{13}C NMR spectra on going from 2 to the violet polymer.[23] There are slight changes in the chemical shifts, the relative intensities of the lines are altered noticeably, and, most importantly, two new peaks appear at δ 150.0 and 145.1. The latter can be reasonably assigned to the alkene carbons of the polyenyne chain, by comparison with model oligo- and polymers[2c,24a] and taking into account the effect of phenyl substitution[24b] and a small cumulenic resonance contribution.[24c] The IR spectrum exhibits an extremely weak C≡C stretching band at 2220 cm^{-1} and a new fingerprint region.[25] The thermal polymerization behavior of 2 can be followed by differential scanning calorimetry (DSC) and thermogravimetric analysis (TGA). DSC shows a sharp exotherm at 145 °C (under N_2) or 155 °C (under air). In air, the initial peak was followed by another steadily increasing exotherm (>250 °C) signaling oxidative decomposition. Finally, TGA (under N_2) revealed a minimal weight loss over the range 135-160 °C (2-3%). At higher temperatures (>250 °C) decomposition was accompanied by slow weight loss reaching 12% at 950 °C.

The described behavior of 2 is typical of diyne monomers undergoing topochemical polymerization. On consideration of the packing diagram in Figure 3 a least motion process suggests the formation of a "trans-trans"-polymer[7a] with the fused annulene moieties adopting an all syn configuration as shown in Figure 5. Conformation of this proposal may be obtained by the synthesis and polymerization of soluble analogs of 2, efforts that are in progress.

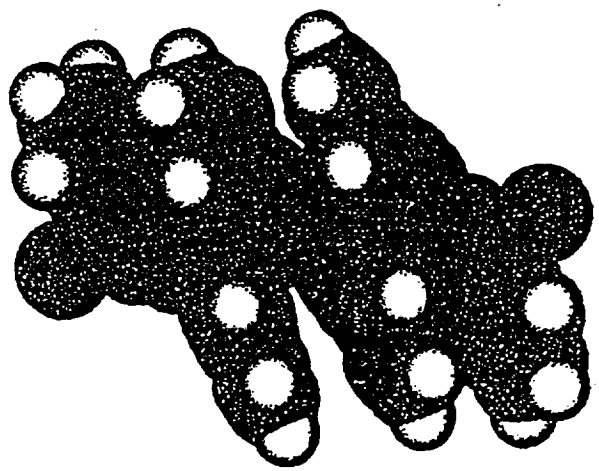

Figure 5. Suggested structure for a trimeric subunit of polymerized 2.

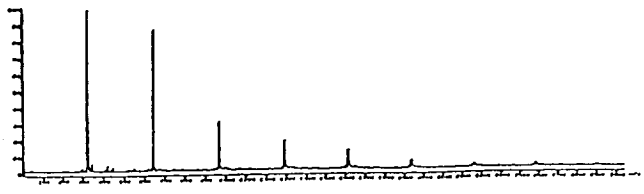

Acknowledgments

This work was supported by the NASA-Lewis Research Center and the National Science Foundation (Grants No. 5-32129 and CHE 9202152). We would like to thank Dr. P. Rinaldi and W. Daunch at the University of Akron for solid state ^{13}C NMR, and Dr. R. Lattimer at BFGoodrich for FDMS spectra. A. J. Matzger was a Syntex predoctoral fellow (1994-1995).

References and Notes

(1) (a) Wegner, G. Z. *Naturforsch.* 1969, *24b*, 824. For selected reviews, see: (b) Kaiser, J.; Wegner, G.; Fischer, E. W. *Isr. J. Chem.* 1972, *10*, 157. (c) Wegner, G. *Pure Appl. Chem.* 1977, *49*, 443. (d) Baughman, R. H.; Chance, R. R. *Ann. N. Y. Acad. Sci.* 1978, *313*, 705. (e) Wegner, G. In *Molecular Metals*; Hatfield, W. E., Ed.; Plenum Press: New York, 1979, p. 209. (f) Bässler, H. *Adv. Polym. Sci.* 1984, *63*, 1. (g) Sixl, H. *Adv.*

1984, *63*, 91. (i) *Polydiacetylenes: Synthesis, Structure, and Electronic Properties*; Bloor, D.; Chance, R. R., Eds.; Jihoff Pub.: 1985. (j) Huntsman, W. D. in *The Chemistry of Triple-Bonded Functional Groups*; Patai, S.; Rappoport, Z. Eds.; Wiley: New York, 1983; Pt. 2, Chap. 22. (k) Shirakawa, H.; Masuda, T.; Takeda, K. in *The Chemistry of Triple-Bonded Functional Groups*; Patai, S., Ed.; Wiley: New York, 1994; Chap. 17.

(2) See, for example: (a) Sauteret, C.; Hermann, J.-P.; Frey, R.; Pradère, F.; Ducuing, J.; Baughman, R. H.; Chance, R. R. *Phys. Rev. Lett.* 1976, *36*, 956. (b) Chance, R. R.; Patel, G. N.; Witt, J. D. *J. Chem. Phys.* 1979, *71*, 206. (c) Chance, R. R. *Macromolecules* 1980, *13*, 396. (d) Thakur, M.; Meyler, S. *Macromolecules* 1985, *18*, 2341. (e) Wudl, F.; Bitter, S. P. *J. Am. Chem. Soc.* 1986, *108*, 4685. (f) *Chem. Eng. News* 1986, *64* (May 5), 33. (g) Butera, R. J.; Simic-Glavaski, B.; Lando, J. B. *Macromolecules* 1990, *23*, 199, 211. (h) Paley, M. S.; Frazier, D. O.; Abeledeyem, H.; McManus, S. P.; Zutaut, S. E. *J. Am. Chem. Soc.* 1992, *114*, 3247. (i) Batchelder, D. N.; Evans, S. D.; Freeman, T. L.; Häussling, L.; Ringsdorf, H.; Wolf, H. *J. Am. Chem. Soc.* 1994, *116*, 1050. (j) Kim, T.; Crooks, R. M.; Tsen, M.; Sun, L. *J. Am. Chem. Soc.* 1995, *117*, 3963. (k) Chan, K. C.; Kim, T.; Schoer, J. K.; Crooks, R. M. *J. Am. Chem. Soc.* 1995, *117*, 5875; and the references therein.

(3) See, for example: (a) Brédas, J. L.; Chance, R. R.; Baughman, R. H.; Silbey, R. *J. Chem. Phys.* 1982, *76*, 3673. (b) Nakanishi, H.; Matsuda, H.; Kato, M. *Mol. Cryst. Liq. Cryst.* 1984, *105*, 77. (c) Se, K.; Ohnuma, H.; Kotaka, T. *Macromolecules* 1984, *17*, 2126. (d) Theocharis, C. R.; Nakanishi, H.; Matsuda, H.; Jones, W.; Thomas, J. M.; Kato, M. *J. Chem. Soc., Chem. Commun.* 1985, 1334; and the references therein.

(4) See, for example: (a) Eichele, H.; Schwoerer, M.; Huber, R.; Bloor, D. *Chem. Phys. Lett.* 1976, *42*, 342. (b) Chance, R. R.; Patel, G. N.; Turi, E. A.; Khanna, Y. P. *J. Am. Chem. Soc.* 1978, *100*, 1307. (c) Baughman, R. H. *J. Chem. Phys.* 1978, *68*, 3110. (d) Chance, R. R.; Patel, G. N. *J. Polym. Sci., Polym. Phys. Ed.* 1978, *16*, 859. (e) Sixl, H.; Neumann, W. *Mol. Cryst. Liq. Cryst.* 1984, *105*, 41.

(5) (a) Wegner, G. *Polym. Lett.* 1971, *9*, 133. (b) Orchard, B. J.; Tripathy, S. K. *Macromolecules* 1986, *19*, 1844. (c) Matsuda, H.; Nakanishi, H.; Kato, S.-I.; Kato, M. *J. Polym. Sci., Polym. Chem. Ed.* 1987, *25*, 1663. (d) Kim, W. H.; Kodali, N. B.; Kumar, J.; Tripathy, S. K. *Macromolecules* 1994, *27*, 1819.

(6) Mayerle, J.J.; Flandera, M. A. *Acta Cryst.* 1978, *B34*, 1374.

(7) (a) For the only extensively studied example, see: Baughman, R. H.; Yee, K. C. *J. Polym. Sci., Polym. Chem. Ed.* 1974, *12*, 2467. Baughman, R. H. *J. Polym. Sci., Polym. Phys. Ed.* 1974, *12*, 1511. Bloor, D. *Chem. Phys. Lett.* 1976, *42*, 174. Bloor, D.; Hersel, W.; Batchelder, D. N. *Chem. Phys. Lett.* 1977, *45*, 411. Day, D.; Lando, J. B. *J. Polym. Sci., Polym. Phys. Ed.* 1978, *16*, 1009. Enkelmann, V.; Graf, H. J. *Acta Cryst.* 1978, *B34*, 3715. (b) For the recently explored "family of exploding [*n*] rotanes," see: de Meijere, A.; Kozhushkov, S.; Haumann, T.; Boese, R.; Puls, C.; Cooney, M. J.; Scott, L. T. *Chem. Eur. J.* 1995, *1*, 124.

(8) (a) Zhou, Q.; Carroll, P.J.; Swager, T. M. *J. Org. Chem.* 1994, *59*, 1294. (b) Guo, L.; Bradshaw, J. D.; Tessier, C. A.; Youngs, W. J. *J. Chem. Soc., Chem. Commun.* 1994, 243. (c) Zhou, Q.; Swager, T. M. *Polym. Prep.* 1993, *34*(1), 193; and the references therein.

(9) Baldwin, K. P.; Bradshaw, J. D.; Tessier, C. A.; Youngs, W. J. *Synlett* 1993, 853.

(10) Hay, A. S. *J. Org. Chem.* 1962, *27*, 3320.

(11) Yellow needles (ethyl acetate-hexanes, 5:95), no m.p. observed; MS(70eV) *m/z* 324 (M^+, 100), 323 (12), 322 (32), 321 (8), 320 (12), 296 (6), 162 (10), 161 (11); ^{13}C NMR (300 MHz, $CDCl_3$): δ = (assignments follow the annulene numbering and the lettering scheme for **2**) 136.0 (C_E), 133.1 (C_A), 129.4 (C_J), 129.2 (C_D), 128.6 (C_B), 128.0 (C_F), 127.9 (C_C), 123.3 (C_I), 122.7 (C_1), 93.76 (C_4), 93.00 (C_3), 85.75 (C_{11}), 80.17 (C_{12}); ^1H NMR (500 MHz, $CDCl_3$): δ = 7.892 (AA' of AA'BB'm, J = 7.93, 1.34, 0.50 Hz, 2H, H_E), 7.860 (A of ABCDm, J = 7.80, 1.19, 0.43 Hz, 2H, H_A), 7.586 (D of ABCDm, J = 7.68, 1.24, 0.43 Hz, 2H, H_D), 7.465 (B of ABCDm, J = 7.80, 7.55, 1.24 Hz, 2H, H_B), 7.432 (BB' of AA'BB'm, J = 7.93, 7.45, 1.34 Hz, 2H, H_F), 7.401 (C of ABCDm, J = 7.68, 7.55, 1.19 Hz, 2H, H_C); UV (CH_2Cl_2): λ_{max} (ε) 254 (4500), 267 (5500), 292 (9500), 299 (9800), 310 (22000), 341 (3000), 351 (3100), 365 (1800) nm; IR (KBr): ν = 3065 (w), 2970 (w), 2930 (w), 2865 (w), 2216 (w), 2150 (w), 1953 (w), 1927 (w), 1887 (w), 1848 (w), 1815 (w), 1736 (m), 1631 (w), 1585 (w), 1552 (m), 1499 (s), 1479 (s), 1453 (m), 1433 (s), 1275 (m), 1242 (m), 1196 (m), 1157 (m), 1104 (s), 953 (m), 880 (m), 755 (vs) cm^{-1}.

(12) 1,2:5,6:9,10-Tribenzo-3,7,11-tridehydro[12]annulene exhibits a very similar spectrum: Campbell, I. D.; Eglinton, G; Henderson, W.; Raphael, R. A. *J. Chem. Soc., Chem. Commun.* 1966, 87.

(13) Balaban, A. T.; Banciu, M.; Ciorba, V. *Annulenes, Benzo-, Hetero-, Homo-Derivatives, and their Valence Isomers*; CRC Press: 1987, Vol. 2, p 147, and the references therein.

(14) (a) Meier, H. *Adv. Strain Org. Chem.* 1991, *1*, 215. (b) Krebs, A.; Wilke, J. *Top. Curr. Chem.* 1984, *109*, 189.

(15) Bax, A.; Summers, M. F. *J. Am. Chem. Soc.* 1986, *108*, 2093.

(16) (a) Vogler, H. *Tetrahedron* 1979, *35*, 657. (b) Mitchell, R. H. *Isr. J. Chem.* 1980, *20*, 294. (c) Huang, N. Z.; Sondheimer, F. *Acc. Chem. Res.* 1982, *15*, 96.

(17) An attempt to use Q values[11] as an additional diagnostic measure of the extent of aromaticity was unsuccessful, e.g. compound (Q value): 1,2-diethynylbenzene (1.079); 1,2:7,8-dibenzo-3,5,9,11-tetradehydro[12]annulene (1.021); 1,2:5,6:9,10-tribenzo-3,7,11-tridehydro[12]annulene (1.039); **2** [1.061 ($H_{E,F}$), 1.038 ($H_{A,B,C}$), 1.018 ($H_{B,C,D}$)]. It is possible that this method is not generally applicable to cycloalkynes of this type, especially when they are strained.[19]

(18) Ref. 13, p. 115.

(19) For the effect of σ-strain on the bond alternation in benzene, see: Glendening, E. D.; Faust, R.; Streitwieser, A.; Vollhardt, K. P. C.; Weinhold. F. *J. Am. Chem. Soc.* 1993, *115*, 10952. Faust, R.; Glendening, E. D.; Streitwieser, A.; Vollhardt, K. P. C. *J. Am. Chem. Soc.* 1992, *114*, 8263.

(20) Crystal data for $C_{26}H_{12}$, monoclinic, $P2_1/c$, a = 16.228 (3), b = 6.308 (1), c = 16.733 (3) Å. β = 99.72 (3)°, Z = 4, V = 1688.3 (5) $Å^3$, D_c = 1.276 g/cm^3, Mo-K_α radiation, λ = 0.71073 Å, $3.5 \leq 2\theta \leq 45°$. Syntex $P2_1$ diffractometer. 2979 reflections were collected of which 2209 unique reflections [$I > 2.0\ \sigma(I)$] were used for refinement (235 parameters), converging to R = 0.0568 and R_w = 0.1337. Further details of the crystal structure investigation may be obtained from the Director of the Cambridge Crystallographic Data Centre, 12 Union Road, Cambridge CB2 1EZ (UK).

(21) (a) Siemens Analytical Instruments, INC., Madison, WI, 1990. (b). SHELXL93, Sheldrick, G. M., University of Göttingen, Göttingen, Germany. (c) R_1 is based on F and R_2 is based on F^2.

(22) For applications in fullerene "coalescence" reactions, see: Creasy, W. R.; Brenna, J. T. *J. Chem. Phys.* 1990, *92*, 2269. Yeretzian, C.; Hansen, K. Diederich, F.; Whetten, R. L. *Nature* 1992, *359*, 44. Cornett, D. S.; Amster, I. J.; Duncan, M. A.; Rao, A. M.; Eklund, P. C. *J. Phys. Chem.* 1993, *97*, 5036. Beck, R. D.; Weis, P.; Bräuchle, G.; Kappes, M. M. *J. Chem. Phys.* 1994, *100*, 262. Hunter, J. M.; Fye, J. L.; Boivin, N. M.; Jarrold, M. F. *J. Phys. Chem.* 1994, *98*, 7440.

(23) CP-MAS ^{13}C NMR (200 MHz) **2**: δ = 136.8, 133.7, 130.1, 124.6, 123.5, 93.9, 87.7, 85.3, 83.2, 80.1; polymer: δ = 150.0, 145.1, 136.9, 129.1, 123.4, 94.0, 87.7, 85.3, 83.2, 80.1.

(24) (a) Nava, A. D.; Thakur, M.; Tonelli, A. E. *Macromolecules* 1990, *23*, 3055 and the references therein. (b) Kalinowski, H. O.; Berger, S.; Braun, S. *^{13}C-NMR-Spektroskopie*; Thieme: Stuttgart, 1984. (c) Nakagawa, M. in *The Chemistry of the Carbon-Carbon Triple Bond*; Patai, S., Ed.; Wiley: New York, 1978; Part 2, Chap. 15. Van Dongen, J. P. C. M.; deBie, M. J.

A.; Steur, R. *Tetrahedron Lett.* 1973, 1371. See also: Myers, A. G.; Finney, N. S. *J. Am. Chem. Soc.* 1992, *114*, 10986.

(25) IR (KBr) polymer: ν = 3059 (m), 2960 (m), 2925 (m), 2861 (m), 2220 (vw), 1719 (s), 1637 (m), 1597 (m), 1449 (s), 1407 (s), 1321 (s), 1256 (s), 1157 (s), 1111 (m), 1025 (w), 927 (w), 874 (w), 749 (vs) cm^{-1}.

J. Org. Chem. 1995, *60*, 1658–1664

Reinvestigation of the Photocyclization of 1,4-Phenylene Bis(phenylmaleic anhydride): Preparation and Structure of [5]Helicene 5,6:9,10-Dianhydride

Aryeh A. Frimer,*,† James D. Kinder,‡ Wiley J. Youngs,§ and Mary Ann B. Meador

Polymer Branch, NASA Lewis Research Center, Cleveland, Ohio 44135, and The Ethel and David Resnick Chair in Active Oxygen Chemistry, Department of Chemistry, Bar-Ilan University, Ramat Gan 52900, Israel

Received November 22, 1994®

The I_2-catalyzed photooxidative cyclization of 1,4-phenylene bis(phenylmaleic anhydride) [PPMA] yields two products in an overall yield approaching 80%. Contrary to a previous report, the major product has been identified by X-ray crystallography as the novel [5]helicene-5,6,9,10-tetracarboxylic 5,6:9,10-dianhydride [HLDA], while the minor product (<5% yield) is the isomeric dibenz[*ah*]-anthracene-5,6,12,13-tetracarboxylic 5,6:12,13-dianhydride [DBAA]. Partial irradiation permits the isolation of the monocyclization intermediate PMPA, which under the photolysis conditions generates the observed dicyclization products. Unlike HLDA, DBAA resists prolonged methanolysis to the corresponding acid esters. This confirms molecular modeling predictions that the 1,6-interaction between the H-4, H-7, H-11, and H-14 aromatic hydrogens and the corresponding neighboring carbonyl oxygens in DBAA inhibit opening of the resulting O–CO anhydride bond. Noteworthy as well is that HLDA, unlike the parent [5]helicene, resists further photocyclization under the reaction conditions to the corresponding benzo[*ghi*]perylene. AM1 semiempirical calculations indicate that, contrary to [5]helicene, there is no buildup of bonding interaction between the designated bonding carbons (C-1 and C-14) as one goes from the HOMO to the corresponding LUMO.

One of the highest priorities of the aerospace industry is the development of high-performance, low-density polymers and polymer matrix composites to serve as metal replacements.[1,2] Over the past two decades,[3] endcap-cross-linked polyimides have proven themselves to be among the best materials for these high temperature applications, combining stability, processibility, and good mechanical properties. Multifaceted and interdisciplinary research continues to improve both the thermooxidative stability and performance of these organic materials.[4–7]

Our own research focus in this area[8–10] has been in improving thermooxidative stability of the polyimide system as a whole by stabilizing the most thermally labile bond therein, presumably the nitrogen–carbon bond of the >NC=O moiety. The dissociation energy of the latter is reported to be somewhere around 65 kcal/mol[11] or perhaps even as low as a mere 50 kcal/mol.[12] In light of this, our attention was drawn to work by Fields and colleagues[13–15] who reported in this journal[15] that I_2-catalyzed photooxidative cyclization[16] (*vide infra*) of the new dianhydride 1,4-phenylene bis(phenylmaleic anhydride) [PPMA] yields the corresponding fully cyclized analog, dibenz[*ah*]anthracene-5,6,12,13-tetracarboxylic 5,6:12,13-dianhydride (DBAA, eq 1).

We noted that in the polyaromatic compound DBAA, the 1,6-interaction between the H-4, H-7, H-11, and H-14 aromatic hydrogens and the corresponding neighboring carbonyl oxygens are expected to inhibit opening of the resulting imide ring (eq 1). H-7 and H-14 are also

* Address correspondence to this author at Bar Ilan University. Tel.: 972-3-5318610. Fax: 972-3-5351250. E-mail: f66235%barilan.bitnet@vm.tau.ac.il.

† NRC-NASA Lewis Senior Research Associate, 1990–1995.

‡ NRC-NASA Lewis Research Associate, 1992–1995.

§ Department of Chemistry, The University of Akron, Akron, OH.

® Abstract published in *Advance ACS Abstracts*, February 15, 1995.

(1) Cassidy, P. E. *Thermally Stable Polymers*; Marcel Dekker: New York, 1980.

(2) See the collection of papers in: *Resins for Aerospace*; ACS Symposium Series No. 132; American Chemical Society: Washington DC, 1980.

(3) Serafini, T. T.; Delvigs, P.; Lightsey. G. R. *J. Appl. Polym. Sci.* **1972**, 16, 905–915.

(4) Meador, M. A.; Cavano, P. J.; Malarik, D. C. In *Structural Composites: Design and Processing Technologies*; Proceedings of the Sixth Annual ASM/ESD Advanced Composites Conference, Detroit, MI, 8–11 Oct 1990; pp 529–539.

(5) Serafini, T. T.; Vannucci, R. D.; Alston, W. B. *Second Generation PMR Polyimides*, NASA TM X-71894.

(6) Vannucci, R. D.; Malarik, D. C.; Papadapoulos, D. S.; Waters, J. F. *Advanced Materials: Looking Ahead to the 21st Century*. Proceedings of the 22nd International SAMPE Technical Conference, Boston, MA, Nov 6–8, 1990, pp 175–185. Also NASA TM 103233.

(7) Bowles, K. *Materials-Process: The Intercept Point*. Proceedings of the 20th International SAMPE Technical Conference, Minneapolis, MN, Sep 27–29, 1988, pp 552–561. Also NASA TM 100922.

(8) Frimer, A. A.; Cavano, P. J. In *Polyimides: Materials, Characterization and Application*. Proceedings of The Fourth International Conference on Polyimides, Feger, C., Ed.; Society of Plastic Engineers, 1991, pp 17–20. Also NASA Technical Memorandum 105335, pp 1–5 (1991).

(9) (a) Frimer, A. A.; Cavano, P. J. In *HITEMP Review 1991: Advanced High Temperature Engine Materials Technology Program*; Gray, H. R., Ginty, C. A., Eds.; NASA CP-10082, 1991; pp 12-1–12-13. (b) Frimer, A. A.; Cavano, P. J.; Alston W. B.; Serrano, A. In *HITEMP Review 1992: Advanced High Temperature Engine Materials Technology Program; Volume I: Overviews, Fan/Compressor Materials (Polymer Matrix Composites), and Fibers*; Gray, H. R., Ginty, C. A., Eds.; NASA Conference Publication 10104, 1992; pp 14-1–14-15. In this latter paper, the correct identity of the major PPMA photocyclization product had not yet been determined. As a result it was thought to be DBAA, when in fact it is HLDA (*vide infra*).

(10) Frimer, A. A.; Cavano, P. J. In *Advances in Polyimide Science and Technology*; Feger, C., Ed.; Technomic Publishing Co.: Lancaster, PA, 1993; pp 41–54.

(11) Jellinek, H. H. G.; Dunkle, S. R. In *Degradation and Stabilization of Polymers*; Jellinek, H. H. G., Ed.; Elsevier: New York, 1983; pp 66–161. See especially pp 75, 77, and 103ff.

(12) Ranby, B.; Rabeck, J. F. *Photodegradation, Photo-oxidation and Photostabilization of Polymers*; Wiley: New York, 1975; p 236.

(13) Fields, E. K.; Winzenberg, M. L.; Behrend, S. J. *Disubstituted Maleic Anhydrides*, U. S. Patent no. 4596867, June 24, 1986.

(14) Fields, E. K.; Winzenberg, M. L.; Behrend, S. J. *Disubstituted Maleic Anhydrides*, U. S. Patent no. 4638072, Jan 20, 1987.

(15) Fields, E. K.; Behrend, S. J.; Meyerson, S.; Winzenberg, M. L.; Ortega, B. R.; Hall, H. K., Jr. *J. Org. Chem.* **1990**, 55, 5165–5170.

(16) Mallory, F. B.; Mallory, C. W. *Org. React.* **1984**, *30*, 1–456.

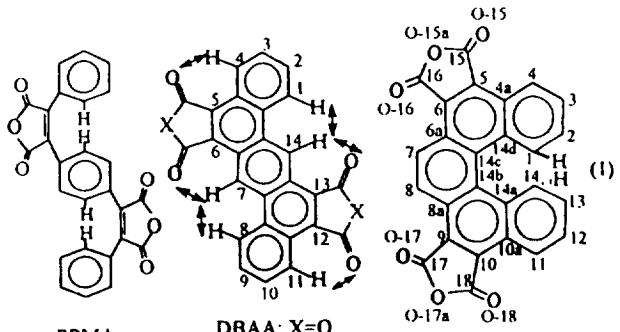

(1)

expected to feel further steric pressure from H-1 and H-8, which would further counter any opening or stretching of the imide N–CO bond. We hoped that this combined buttressing effect would serve to improve the TOS of polyimides derived therefrom. Our structural predictions agreed with molecular modeling studies.[17] These indicated that DBAA should be an essentially planar and rigid molecule (Figure 1); nevertheless, H-14 and H-7 are slightly twisted away from the carbonyl,[18] reflecting the aforementioned 1,6-interactions.

As reported below, our reinvestigation of the photolysis of PPMA has led us to the conclusion that Fields and coworkers[13-15] erred in identifying DBAA as the major product of this reaction. While DBAA is formed in low yield, the main product of the photolysis is the isomeric [5]helicene-5,6,9,10-tetracarboxylic 5,6:9,10-dianhydride [HLDA] (eq 1). The preparation and characterization of this novel helicene dianhydride is described herein.

Results And Discussion

A. Photooxidative Cyclization of PPMA. *cis*-Stilbene moieties are known to undergo a reversible photocyclization to the corresponding *trans*-4a,4b-dihydrophenanthrene. The latter can be oxidized to the corresponding phenanthrene by hydrogen acceptors such as iodine and/or oxygen (eq 2). In systems where more

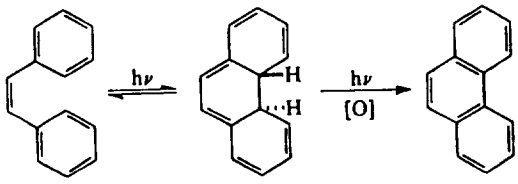

(2)

than one stilbene moiety is present, two consecutive cyclizations can occur.[19]

Fields reports that PPMA, which contains two such stilbene systems, undergoes this double transformation, yielding yellow powder in a 25–30% yield.[13-15] We have found that this yield can be raised to as much as 88%, when the Katz propylene oxide modification is utilized

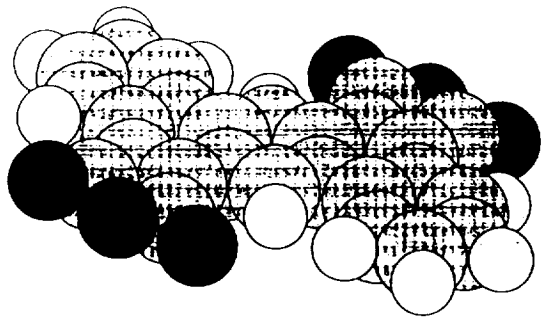

Figure 1. HyperChem space-filling model of DBAA.

(eq 3),[20,21] and have also isolated a small amount (<5%)

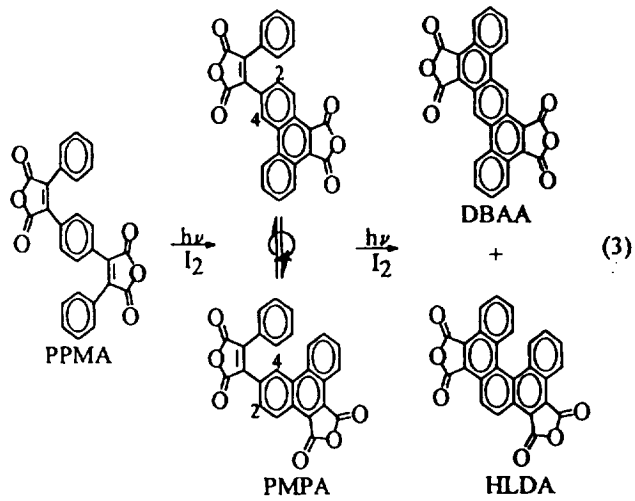

(3)

of isomeric material. The HRMS and elemental analysis of both isomers correspond to a molecular formula of $C_{26}H_{10}O_6$, indicating that a double cyclization has occurred in both cases. Partial irradiation permits the isolation of the monocyclization intermediate 3-(phenylmaleic anhydride)phenanthrene-9,10-dicarboxylic anhydride [PMPA], which under the photolysis conditions generates the observed dicyclization products (eq 3).

The formation of two dicyclization isomers presumably results from the closure of the *ortho* carbon of the PMPA phenyl with either the C-2 or C-4 of the PMPA phenanthrene (eq 3). In the former case, the aforementioned flat and rigid dibenzanthracene system (DBAA) is formed. In the latter instance, however, a five-ring *ortho*-bonded helical structure results; hence, the name [5]helicene dianhydride (HLDA; see also eq 1). Although helicenes[19,22] are well known, no dianhydrides have yet been reported. Molecular modeling studies[23] (Figure 2) predict HLDA to be helical in structure and twisted out of planarity because of the H-1/H-14 steric interaction (see eq 1). The helicene structure is, furthermore, predicted to be about 10 kcal/mol less stable than the isomeric DBAA.

(17) Autodesk HyperChem 3, AM1 semiempirical calculation; results were confirmed in several substrates by related calculations using Tripos Sybyl 5.4 Molecular Modeling Program.

(18) The calculated heat of formation of the geometry-optimized DBAA is −80.968 kcal/mol (gradient 0.036 kcal/mol/Å) as compared to a value of −46.631 (gradient 20.112) for the completely flat analog. The HyperChem geometry optimization introduces a slight twist throughout the ring system so that the H-7 hydrogen is bent down below the ring plane while H-8 and the carbonyl are bent up creating a dihedral angle of ca. 0.035° in each case. The dihedral angle between H-7 and H-14 is ca. 0.32°.

(19) Mallory, F. B.; Mallory, C. W. *Org. React.* **1984**, *30*, 1–456.

(20) Liu, L.; B. Yang; Katz, T. J.; Pointdexter, M. K. *J. Org. Chem.* **1991**, *56*, 3769–3775.

(21) Liu, L.; Katz, T. J. *Tetrahedron Lett.* **1991**, *32*, 6831–6834.

(22) (a) Laarhoven, W. H.; Prinsen, W. J. C. *Top. Curr. Chem.* **1984**, *125* (Stereochemistry), 63–130. (b) Martin, R. H. *Angew. Chem., Int. Ed Engl.* **1974**, *13*, 649–660. (c) The numbering of the helicene carbons follows the convention first proposed: Newman, M. S.; Lednicer, D. *J. Am. Chem. Soc.* **1956**, *78*, 4765–4770. (d) Kuroda, R. *J. Chem. Soc., Perkin Trans. 2* **1982**, 789–794.

(23) The calculated heat of formation of the geometry optimized HLDA (Figure 2) is −70.936 kcal/mol (gradient 0.042 kcal/mol/Å). This should be compared to a value of +1725.920 (gradient 484.489) for the completely flat analog.

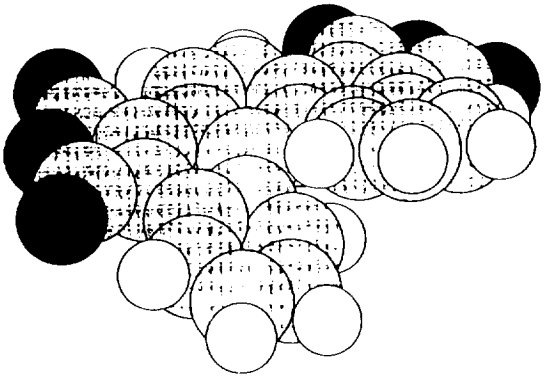

Figure 2. HyperChem space-filling model of HLDA.

Table 1. Selected Physical Data on HLDA Precursors and Isomers

	PPMA	PMPA	HLDA (major)	DBAA (minor)
DSC[a]	261	312	403[b]	496 °C
FTIR (C=O)	1830	1841	1840	1842 cm^{-1}
				1819 cm^{-1}
	1765	1770	1769	1755 cm^{-1}
NMR[c] (C=O)	164	164	163	164 ppm
			161	
MS (M^+)	422	420	418	418 amu

[a] N_2 200 psi. Modulated DSC confirms that the corresponding melt endotherms are reversible. [b] The mp determined by TMA on a pressed pellet was 400 °C. [c] For the purpose of comparison, the solid state ^{13}C NMR carbonyl absorptions of 2,3-diphenylmaleic anhydride (DPMA, Aldrich) and the corresponding photocyclized analog, phenanthrene anhydride (PA, see experimental) are 164.74 and 160.31, respectively.

B. Identification and Characterization of HLDA and DBAA. The question remains: which is the major isomer, HLDA or DBAA? Fields *et al.*[15] reports observing only one isomer and identified it as DBAA. His suggestion is based on his expectation that HLDA should show a large [M − $2C_2O_3$ − H_2] peak as a result of a facile loss of the two anhydride moieties followed by further cyclization between C-1 and C-14. However, in our hands both isomers have [M − $2C_2O_3$ − H_2] peaks with an amplitude of 1/4 of the [M − $2C_2O_3$] peak.

As Table 1 reveals, the remaining spectral data as well is of little assistance in answering this question. Since both isomers are insoluble in most organic solvents, typical NMR characterization was precluded. Solid state ^{13}C NMR was performed revealing in both cases three groups of broad absorptions: carbonyl (170−160 ppm), quarternary aromatic (130−140 ppm), and CH aromatic (120−130 ppm) (see Figure 3). Although there are indeed differences in the spectra of the two isomers (see Figure 3 and Table 1), each could well correspond to either structure. The melting points of both isomers are above 400 °C and were measured by differential scanning calorimetry (DSC). The lower melting point of the major isomer argues in favor of it being the less compactly packed HLDA, while the greater stability of DBAA might suggest that it is the major product. In short, the aforementioned data were not the type on which a solid characterization could be based.

(24) Surprisingly, however, the DSC-determined onset of melting for the crystalline samples is about 8−10 °C *lower* than the amorphous analog, though the maxima remain unchanged. Similarly, the TGA-determined T_d (onset) of the crystalline DBAA is as much as 70 °C *lower* than the corresponding amorphous analog (see the Experimental Section). TGA, DSC, or FTIR (interactive subtraction) of the recrystallized HLDA gave no indication of the presence of residual NMP. These

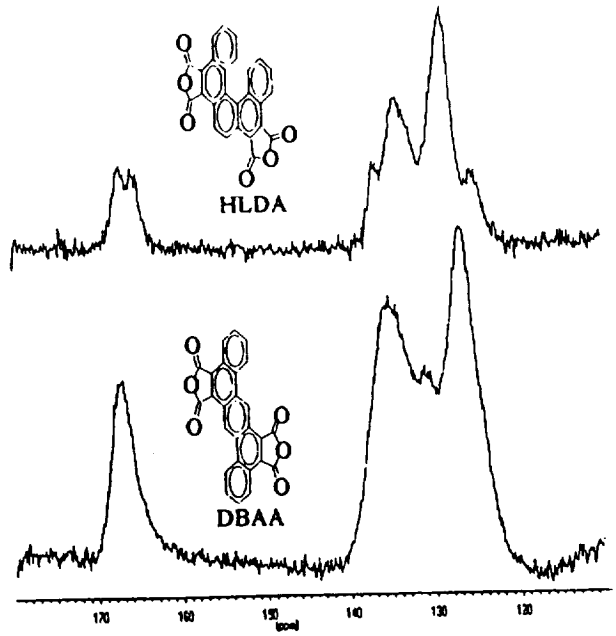

Figure 3. Solid state ^{13}C NMR spectra of HLDA and DBAA.

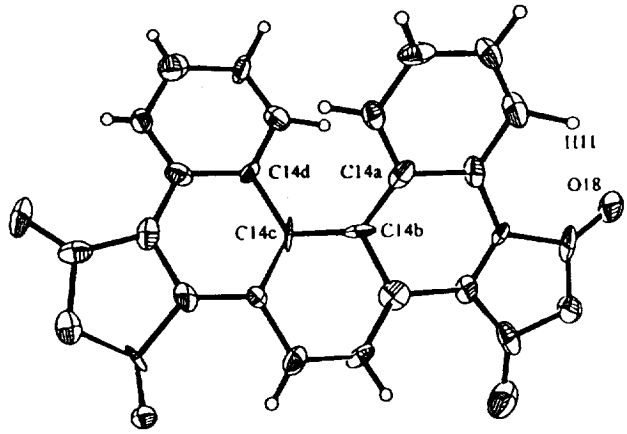

Figure 4. Thermal ellipsoid labeling diagram of HLDA. (The thermal ellipsoids were drawn at the 50% level.)

We did discover that the major isomer could be recrystallized from hot *N*-methylpyrrolidone (NMP) as yellow cubes.[24] X-ray crystallography easily supplied the desired information, demonstrating conclusively that the major isomer was HLDA. The crystal structure showing the thermal ellipsoids is given in Figure 4. The torsional angle defined by carbons 14a-14d is 32.8° (Figure 5). This is a bit larger than the value of 30° that Kuroda found for [5]helicene.[22d] The distances (in Å) between a carbonyl oxygen and the closest aromatic hydrogen are as follows: O_{18}−H_{11} = 2.243, O_{15}−H_4 = 2.793, O_{16}−H_7 = 2.501, O_{17}−H_8 = 2.510 or an average distance of 2.512 Å. These distances are not particularly short, and hence, we need not expect these hydrogens to effect a steric inhibition to anhydride opening of the type predicted for DBAA. Analysis of the packing diagram for HLDA revealed three short intermolecular hydrogen bonding interactions (Figure 6).

The preferential formation of HLDA is consistent with an earlier report of Laarhoven[25] that *p*-distyrylbenzene photocyclizes to 3-styrylphenanthrene (eq 4). Further

(25) Laarhoven, W. H.; Cuppen, Th. J. H. M.; Nivard, R. J. F. *Tetrahedron* 1970, *26*, 1069−1083.

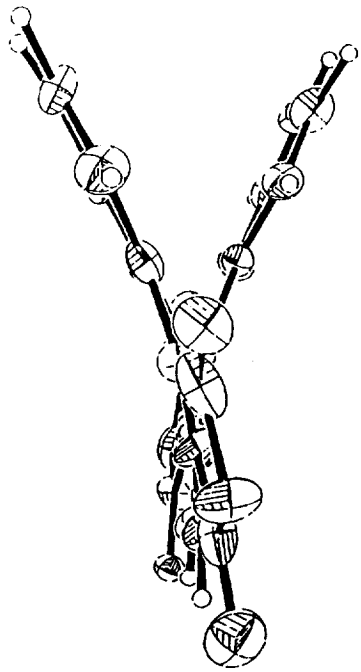

Figure 5. Diagram showing the torsional angle in HLDA.

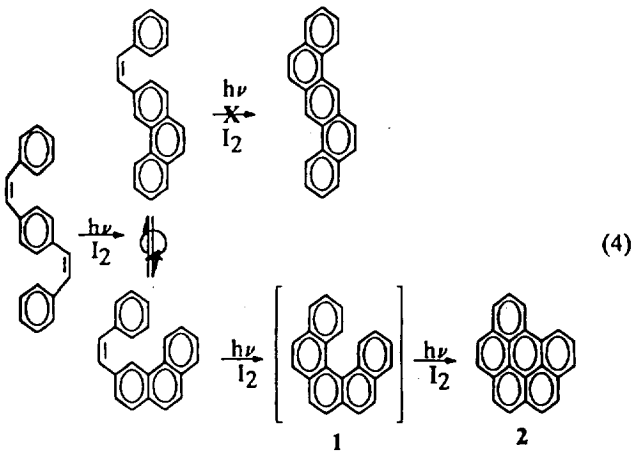

(4)

cyclization of the latter could theoretically yield either [5]helicene (1) or dibenzanthracene. In fact, only a single product is observed which was identified as benzo[*cde*]-perylene 2 and which is the known photodehydrocyclization product of 1.[26] The reason for the preferential formation of [5]helicene (1) has been rationalized in terms of a series of selection rules.[22,25,26a,27] An extensive theoretical study is currently underway to determine their applicability to the PPMA to HLDA transformation as well, and in particular the effect of the anhydride moieties on the molecular orbital system.

C. Methanolysis of HLDA and DBAA. When crude HLDA (containing <5% DBAA) from the photolysis was suspended in refluxing methanol (ca. 0.1 M) for 1 week, approximately 40% of the dianhydride dissolved. More dissolved if the initial methanol to HLDA ratio was larger. The resulting orange-yellow solution was filtered, and the undissolved precipitate proved to be HLDA substantially enriched in DBAA. (Indeed, repeated methanolysis of this sample ultimately yielded *pure DBAA*.) Evaporation of the filtrate gave a yellow solid which, unlike HLDA, was soluble in acetone and $CHCl_3$. [Interestingly, the $CHCl_3$ solutions slowly (within 1 h) precipitated *pure HLDA*, undoubtedly by acid-mediated recyclization.] The mass spectrum of the yellow solid was essentially the same as that of HLDA, confirming the facile loss of methanol. The FTIR spectrum too was similar to that of HLDA but contained extra distinctive peaks at 3453 (br, s, acid OH), 1729 (s, acid C=O), and 1444 (m, acid COH bending). The ^1H NMR spectrum was quite complicated in the aromatic region but revealed methoxy peaks at 4.06, 4.08, and 4.10 ppm. The ^{13}C NMR was equally complicated but clearly indicated the presence of several sets of carbonyls at ca. 163 (anhydride), 168 (ester), and 171 (acid) ppm and methoxy carbons at ca. 53 ppm. While we cannot make a definite identification of the components of the product mixture, the chemical and physical data strongly support the suggestion that the mixture is comprised of the various isomers resulting from the methanolysis of one (two isomers) or both (three isomers) of the anhydrides of HLDA (see eq 5).[28] We will refer to this mixture of HLDA acid esters as HLDE.

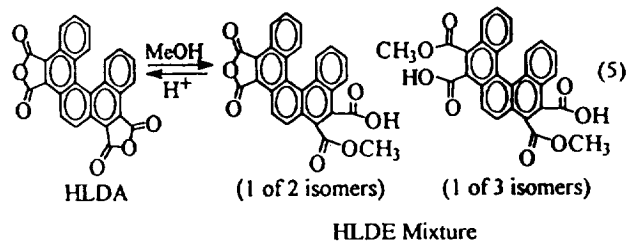

(5)

The fact that DBAA, in contradistinction to HLDA, is totally resistant to methanolysis, lends credence to the correctness of the opening hypothesis of this paper. Namely, that the scission of the O–CO bond (be it solvolytic or thermal) in this polyaromatic compound is strongly inhibited by the 1,6-interaction between the H-4, H-7, H-11, and H-14 aromatic hydrogens (eq 1). The role of such steric pressure in stabilizing polyimides will be explored in future work.

D. [5]Helicene Photochemistry. Perhaps the most intriguing result is that HLDA, in contrast to the corresponding [5]helicene (1, eq 4),[19,20] was not photocyclized further under the reaction conditions to the corresponding benzo[*ghi*]perylene 3 (eq 6). Such a lack of reactivity is not unprecedented, since hydrocarbons 4[27d] and 6,[29] for example, also fail to undergo oxidative photocyclization (eqs 7 and 8).

The explanation given for the differing behaviors of 4 and 6 as compared to 1 relates to the fact that, in the first step of such photocyclizations, a HOMO to LUMO excitation occurs. Focusing on the coefficients of the two interior carbons, closure will be encouraged upon irradiation if the LUMO has greater bonding character than the corresponding HOMO.[22,27d,29] Indeed, AM1 semiempirical

(26) (a) Scholtz, M.; Muhlstadt, M.; Dietz, F. *Tetrahedron* **1968**, 6845–6849. (b) See also refs 19 and 20.

(27) (a) Laarhoven, W. H.; Cuppen, Th. J. H. M.; Nivard, R. J. F. *Rec. Trav. Chim, Pays-Bas* **1968**, *87*, 687–698. (b) Laarhoven, W. H.; Cuppen, Th. J. H. M.; Nivard, R. J. F. *Tetrahedron* **1970**, *26*, 4865–4881. (c) Laarhoven, W. H.; Cuppen, Th. J. H. M.; Nivard, R. J. F. *Tetrahedron* **1970**, *26*, 1069–1083. (d) Tinnemans, A. H. A.; Laarhoven, W. H.; Sharafi-Ozeri, S.; Muszkat, K. A. *Rec. Trav. Chim, Pays-Bas* **1975**, *94*, 239–243.

(28) Mass spectral data suggests that at very long reflux times (~30 d) a diester anhydride and a tetraester are the primary products.

(29) Mallory, F. B.; Mallory, C. W. Unpublished results cited in ref 19, p 20.

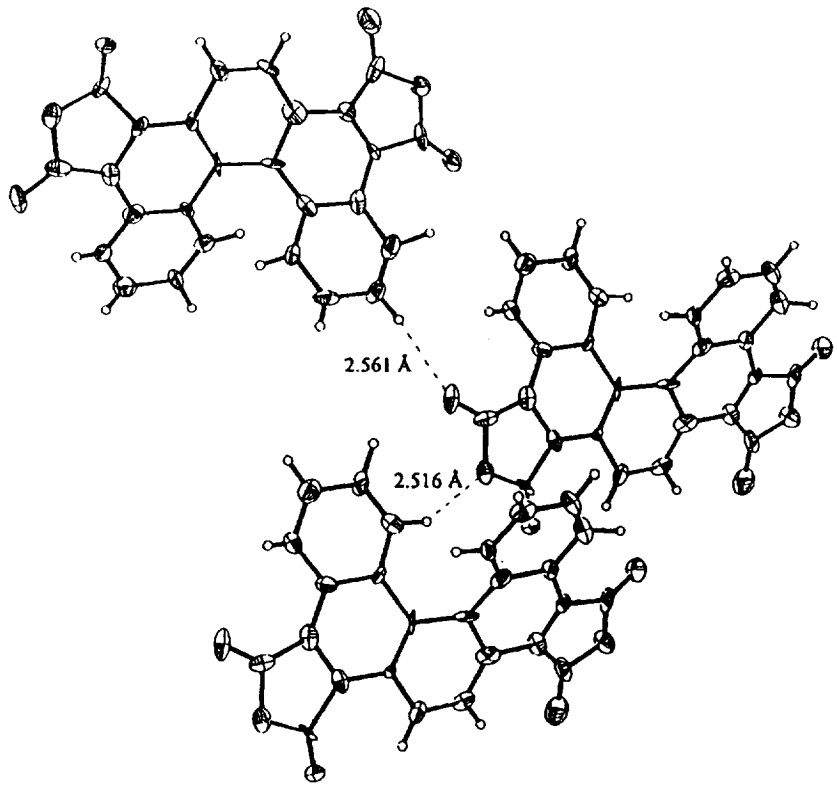

Figure 6. Packing diagram of HLDA showing the intermolecular hydrogen bonding interactions.

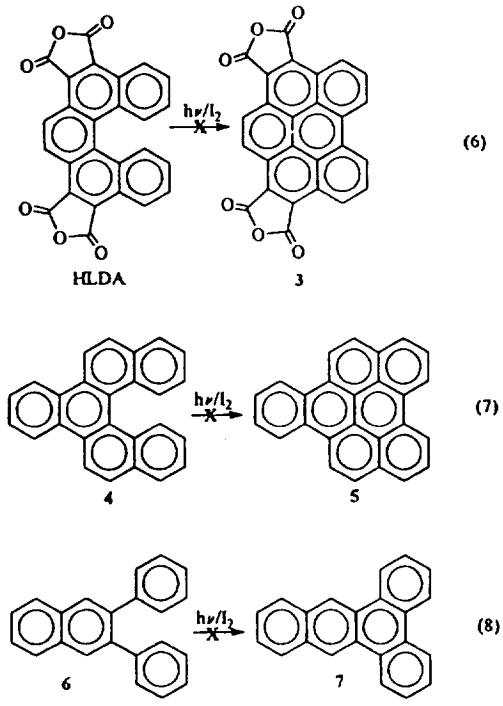

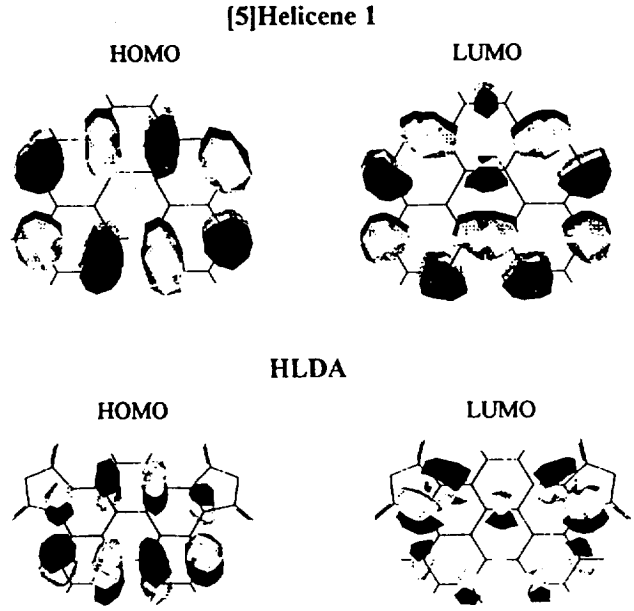

Figure 7. HOMO and LUMO orbitals of [5]Helicene 1 and HLDA.

calculations[30] predict that in the HOMO of both [5]-helicene (**1**) and HLDA there is an antibonding interaction between the two interior bonding carbons C-1 and C-14 (Figure 7). In the case of **1**, however, while the corresponding LUMO orbital has a sizable bonding interaction; there is no such interaction in the LUMO of HLDA.

(30) Autodesk HyperChem 3, AM1 semiempirical calculations of the orbitals were carried out on flat (non-geometry optimized) models of [5]helicene and HLDA. The molecular orbitals were drawn using Hypercube ChemPlus (Waterloo, Ontario).

Experimental Section

^1H and ^{13}C NMR spectra were obtained on a Bruker AM 300 Fourier transform spectrometer. Solutions were generally prepared in $CDCl_3$ using TMS as the internal standard. Solid samples were run with a high power solid attachment using a side band suppression subroutine for cross-polarization. The solids probe was equipped with a dual-air bearing capable of "magic angle" spinning at rates up to 5 kHz and tunable over the frequency range from ^{14}N to ^{63}Cu. The solids spectra were externally referenced to the carbonyl of glycine (196.1 ppm relative to TMS). All IR spectra were recorded on KBr pellets using a Perkin-Elmer 1750 FTIR. Mass spectral analyses were performed by The Midwest Center for Mass Spectrometry

(Lincoln, NE) using a Kratos MS-50 triple analyzer. Elemental Analyses were performed by Spang Microanalytical Laboratory (Eagle Harbor, MI). Thin layer chromatography (TLC) was carried out on Merck silica gel F_{254} precoated plates. Flash chromatography was performed on Merck silica gel, grade 60, 230–400 mesh, 60 Å. Melting points were determined in a Thomas Hoover capillary melting point apparatus and are uncorrected. Thermogravimetric analyses (TGA) were done on cured resin samples with a Perkin-Elmer TGS-2 (under air with a scan rate of 10 °C/min) using a PL Thermal Sciences (formerly Omnitherm Advantage II) thermal analysis system (TAS). Thermomechanical analyses (TMA) were carried out on cured resin samples with a DuPont Instruments 943 TMA (under air with a scan rate of 10 °C/min) using a PL Thermal Sciences TAS. Differential scanning calorimetry (DSC) was carried out on high melting monomer or imidized molding powder (prepolymer) in a Perkin-Elmer DSC 7 cell (under air or 200 psi N_2; scan rate: 10 °C/min) with a Perkin-Elmer Series 7 TAS. Modulated DSC analysis (for determining the reversibility of transitions) was performed with a Thermal Analysis Instrument (New Castle, DE) Module 2910 modulated DSC (N_2 purge; scan rate: 10 °C/min).

1,4-Phenylene Bis(phenylmaleic anhydride) [PPMA]. PPMA was prepared essentially as described by Fields *et al.*[13-15] from 1,4-phenylenediacetic acid (Aldrich, 145.6 g, 0.75 mol) and sodium benzoyl formate (Aldrich, 258.2 g, 1.5 mol) in 1 L of glacial acetic acid (Fisher) with the following modification of the workup and recrystallization procedure. After 1 h at reflux, the cooled solution was poured into 6 L of water,[13,14] filtered, washed with water, and air dried overnight giving 356 g of brown powder. The crude product was washed four times with cold acetone yielding 3.5 L of a deep brown solution, which upon concentration gave 72 g of impure gold-brown powder (mp 253–255 °C). The remaining undissolved product (approximately 200 g of gold-brown powder) was then heated with 3.5 L of hot acetone yielding a green solution, which upon concentration gave 76 g of semipure brownish gold crystals (mp 260–261 °C). The remaining undissolved lemon-yellow product was dissolved completely in 6 L of hot acetone, which upon concentration gave 107 g of pure fluorescent shiny lemon-yellow platelets (mp 261–262 °C) (ca. 80% yield). We should note that recrystallization of the first two brownish gold fractions yielded purer product of higher mp (up to 261–262 °C) and crystallinity, but despite treatment with charcoal, the brownish-tint remained. PPMA is soluble in acetone, THF, and DMSO,[15] as well as in $CHCl_3$, dioxane, and NMP.

PPMA: ^{1}H NMR ($CDCl_3$) δ 7.61 (bs, 4H, phenylene), 7.57–7.37 (m, 10H, phenyl); ^{13}C NMR ($CDCl_3$) δ 164.391, 164.321, 139.608, 136.568, 131.670, 130.195, 129.773, 129.729, 129.156; ^{13}C NMR (solid) δ 163.58 (CO), 138.59, 135.06, 129.87, 127.93; FTIR (KBr) 1830 (C=O, m), 1765 (C=O, s) cm^{-1}.

Photooxidative Cyclization of PPMA. Formation of HLDA, DBAA, and PMPA. PPMA was photocyclized by modifications of two literature methods: (a) Fields Method.[13-15] A 3 L conical photochemical reactor fitted with a water-jacketed immersion well (containing a 450-W medium-pressure mercury vapor lamp surrounded by a Pyrex filter), a gas inlet tube, and a condenser (leading to a bubbler) was charged with PPMA (50.64 g, 0.12 mol), I_2 (0.24 g, 0.96 mol), and 2.8 L of acetone. The red-brown reaction mixture was magnetically stirred and irradiated under bubbling oxygen. The dull orange-yellow product, which is insoluble in the reaction solvent, tends to coat the immersion well, but can be removed as necessary with a Teflon spatula. The reaction mixture was filtered after 21, 42, and 111 h of irradiation yielding 7.38, 4.90, and 4.10 g, for a total of 16.38 g (0.039 mol, 33% yield) of product. A new portion of I_2 (0.24 g) was added to the reaction solution after each filtration. These first three fractions were identified by their IR spectral data as HLDA of varying purity, containing small (ca. 0–3%) but increasing amounts of DBAA. Further irradiation for an additional 87 h (while adding iodine every 24 h), yielded another 0.56 g (0.0013 mol, 1.1% yield) of a spectrally different product, subsequently identified as DBAA. A pure sample of DBAA was also obtained from repeated methanolysis of the above HLDA fractions (*vide infra*).

(b) Katz Method.[20] The aforementioned 3 L photochemical reactor was charged with PPMA (21 g, 0.05 mol), I_2 (26 g; 0.1 mol), 1.4 L of acetone, and 1.4 L of propylene oxide. The red-brown reaction mixture was flushed with N_2 for 20 min and irradiated under bubbling N_2. Product formed rapidly, and the immersion well had to be cleaned sometimes as often as every 1.5–2 h. After about 10 h of irradiation, the reaction solution had turned green (no I_2 remaining), product formation had essentially ceased, and the product formed had a dull yellow color. (On the basis of DSC data, the latter is primarily PMPA. Indeed, pure PMPA can be obtained by filtering the reaction solution every few hours so that photocyclization does not go to completion.) An additional portion of I_2 (12.8 g) was added, and the irradiation was continued (ca. 20 h) until the immersion well remained free of product for 2 h. The product, which now has the orange-yellow HLDA color, was gravity filtered, washed several times with acetone, and dried overnight in a vacuum oven at 200 °C to give an 88% yield of HLDA (18.4 g; 0.044 mol). DBAA and HLDA are insoluble in acetone, pyridine, $CHCl_3$, ethanol, ether, dioxane, DMF, DMAC, and HOAc. HLDA, and to a much lesser extent DBAA, is partially soluble in hot NMP (*vide infra*).

Crude HLDA (1 g from photolysis, contaminated with a few percent of DBAA) was partially dissolved in hot NMP (40 mL). The deep black/brown-green solution was filtered and concentrated down to 13 mL. [IR and DSC indicated that the undissolved material was a mixture of DBAA and HLDA.] The filtrate was allowed to cool slowly, with the concomitant formation of small green crystals (0.42 g); under a microscope, the latter proved to be yellow cubes. The mother liquor was concentrated down to ca. 7 mL, and a second crop was obtained (0.19 g; total of 0.61 g). The crystals were washed with cold acetone and dried at 200 °C overnight and 3 h at 260 °C to remove any residual NMP. TGA, DSC, or FTIR (interactive subtraction) of the recrystallized HLDA gave no indication of the presence of residual NMP. By comparison, DBAA is sparingly soluble in NMP, and repeated attempts to recrystallize it from this solvent failed. Instead, a fine brown powder was obtained, which was identified by IR and DSC as DBAA.

The DSC trace of HLDA is highly dependent on the method of analysis. Under 200 psi of N_2 pressure (see Table 1), the melt endotherm [402.5 (onset), 410.2 (max) °C] is followed by an exotherm [418.6 (onset), 445.6 (max) °C]. On the other hand, when the DSC is modulated[31] and measured under N_2 purge (30 cm^3/min), one observes a reversible melt endotherm [394.7 (onset), 412.9 (max) °C] accompanied by a second overlapping nonreversible endotherm [399.5 (onset), 426.1 (max) °C]. Furthermore, during the latter measurement, sublimed HLDA collects on the lid of the DSC chamber. We interpret the above data as follows: at *ca.* 400 °C and ambient pressure, HLDA melts (reversible transition) and volatilizes (nonreversible sublimation); however, at 200 psi, volatilization is inhibited and the melt is followed at around 420 °C by the onset of decomposition. Similarly, modulated DSC under N_2 purge of DBAA reveals that the reversible melt endotherm [489.4 (onset), 510.9 (max) °C] is accompanied by a large irreversible volatilization endotherm [470.0 (onset), 509.8 (max) °C]; as before, during the measurement, sublimed HLDA collects on the lid of the DSC chamber.

HLDA (amorphous powder from photolysis): DSC (N_2 200 psi) typically 402.6 (onset), 412.6 (endo, max) °C [though some samples have shown values as high as 409.8 (onset), 413.8 (endo, max)], 418.6 (onset), 445.6 (exo, max) °C; Modulated DSC (amorphous, N_2 purge, 30 cm^3/min) *normal heat-flow* 394.7 (onset), 412.9 (endo, max), 426.1 (endo, max) °C, *nonreversible heat-flow* 399.5 (onset), 426.2 (endo, max) °C, *reversible heat-flow* 394.7 (onset), 412.9 (endo, max) °C; TMA (pressed pellet, static air) 399.55 °C; TGA: T_d = 495.5 °C; mp

(31) Modulated or oscillating DSC is a new technique which permits the determination of reversible and nonreversible transitions. For recent references, see: (a) Reading, M.; Elliott, D.; Hill, V. L. *J. Therm. Anal.* **1993**, *40*, 949–955. (b) Cesaro, A.; Navarini, L.; Pepi, R. *Thermochim. Acta* **1993**, *227*, 157–166. (c) Reading, M. *Trends Polym. Sci.* **1993**, *1*, 248–253. (d) Sauerbrunn, S. R.; Crowe, B. S.; Reading, M. *Polym. Mater. Sci.* **1993**, *68*, 269–271. (e) Sichina, W. J. *Am. Lab.* **1993**, *25*, 26–30.

(TMA, static air) 399.6 °C; ^{13}C NMR (solid) δ 162.74 (C=O), 161.17 (C=O), 132.04, 130.22, 129.03 and 125.30 (aromatic); FTIR (KBr, %T) 1840.3 (C=O, 56), 1769.0 (C=O, 33), 1255.8 (82), 1196.0 (62), 1176.7 (82), 1163.2 (67), 1151.7 (78), 906.6 (70), 798.6 (78), 777.4 (81), 736.9 (90) cm^{-1}; HRMS calcd ($C_{26}H_{10}O_6$, M^+) 418.0477, obsd 418.0489 (16.02); calcd ($C_{23}H_{10}O_3$, M − C_2O_3) 346.0629, obsd 346.0630 (13.67); calcd ($C_{22}H_{10}$, M − $2C_2O_3$) 274.0782, obsd 274.0782 (16.29), calcd ($C_{22}H_8$, M − $2C_2O_3$ − 2H) 272.0626, obsd 274.0624 (4.69). Anal. Calcd ($C_{26}H_{10}O_6$): C, 74.64, H, 2.41. Found: C, 74.74; H, 2.51.

HLDA (after NMP recrystallization): DSC (N_2 200 psi) 393.9 (onset), 406.1 (endo, max), 411.6 (onset), 440.6 (exo, max) °C; Modulated DSC (N_2 purge, 30 cm^3/min) *normal heat-flow* 389.2 (onset), 412.1 (endo, max), 428.3 (endo, max) °C, *nonreversible heat-flow* 394.2 (onset), 429.9 (endo, max) °C, *reversible heat-flow* 385.1 (onset), 412.0 (endo, max) °C; TGA: T_d = 422.5 °C with second inflection at 489 °C.

DBAA: DSC (N_2 200 psi) 496.4 (onset), 506.1 (endo, max) 527.3 (endo, max) °C; Modulated DSC (N_2 purge, 30 cm^3/min) *normal heat-flow* 468.0 (onset), 509.6 (endo, max) °C, *nonreversible heat-flow* 470.0 (onset), 509.8 (endo, max) °C, *reversible heat-flow* 489.4 (onset), 510.9 (endo, max), 519.29 (endo, max) °C; ^{13}C NMR (solid) δ 163.50 (C=O), 132.02 (aromatic), 122.98 (aromatic); FTIR (KBr, %T) 1842.5 (43), 1819.10 (58) and 1755.45 (C=O, 60), 1257.75 (58), 1184.44 (33), 1167.08 (40), 910.52 (41), 781.27 (48) cm^{-1}; HRMS: calcd ($C_{26}H_{10}O_6$, M^+) 418.0477, obsd 418.0469 (100); calcd ($C_{23}H_{10}O_3$, M − C_2O_3) 346.0629, obsd 346.0626 (49.01); calcd ($C_{22}H_{10}$, M − $2C_2O_3$) 274.0782, obsd 274.0779 (36.82); calcd ($C_{22}H_8$, M − $2C_2O_3$ − 2H) 272.0626, obsd 274.0621 (9.81). Anal. Calcd ($C_{26}H_{10}O_6$): C, 74.64; H, 2.41. Found: C, 75.04; H, 2.40.

PMPA: mp (DSC, N_2 200 psi) 312.1 (onset), 315.8 (max) °C; ^{13}C NMR (solid) δ 163.87 (CO), 131.5 (aromatic), 125.89 (aromatic); FTIR (KBr, %T) 1841 (C=O, 17), 1770 (C=O, 3), 1627 (conjugated C=C, 42.8), 1256 (37), 1195 (17), 1176 (36), 1163 (20), 1151 (33), 907 (20), 800 (25), 779 (24) cm^{-1}; HRMS calcd ($C_{26}H_{12}O_6$, M^+) 420.0634, obsd 420.0647. MS (EI, 70 eV, 300 °C) *m/e* 420 (M^+, 100), 348 (M − CO − CO_2, 81.90), 276 (M − $2C_2O_3$, 85.20), 274 (M − $2C_2O_3$ − H_2, 46.86).

Photooxidative Cyclization of Diphenylmaleic Anhydride (DPMA). Formation of Phenanthrene-9,10-dicarboxylic Anhydride (PDA). Following the Katz method,[20] a 500 mL photochemical reactor (see previous section) was charged with DPMA (Aldrich, 5 g, 20 mmol), I_2 (5 g, 39 mmol), acetone (250 mL), and propylene oxide (250 mL). The reactor was flushed for 20 min with N_2 prior to irradiating the reaction mixture with a 450-W Hanovia lamp. After 2.5 h, the I_2 color had disappeared and substantial precipitate formed. (In contradistinction to the above photolysis of PPMA, no solid attached itself to the immersion well.) Additional I_2 (2 g) was added and the irradiation continued for another 1.5 h. The precipitate was filtered, washed three times with acetone, and dried in a 90 °C vacuum oven to give 3.85 g (15.5 mmol, 78% yield) of PDA. The IR, UV, and ^1H NMR spectra (DMSO 140 °C) have been reported.[32-34]

DPMA: ^{13}C NMR (solid) δ 164.74 (C=O), 137.83, 130.05 and 126.37 (aromatic).

PDA: mp (DSC, static air) 316.89 (onset), 318.01 (max) (lit.[35] mp 317 °C); ^{13}C NMR (solid) δ 160.35 (C=O), 132.10, 131.10, 125.20 and 124.41 (aromatic).

Methanolysis of HLDA. HLDE. HLDA (7.8 g, 18.6 mmol) was suspended in 180 mL of methanol and refluxed for 7 d. The resulting orange-yellow solution was filtered, and the undissolved precipitate (4.7 g, 11.2 mmol; 40% dissolved) proved to be HLDA substantially enriched in DBAA. (Repeated methanolysis of this sample ultimately yielded pure DBAA.) Rotary evaporation of the filtrate yielded a yellow solid. The latter was identified as a mixture of the isomers of the monoanhydride acid ester of HLDA and the diacid diesters (HLDE).

HLDE: ^1H NMR ($CDCl_3$) δ 9.0−8.6, 8.4−8.2, 8.2−7.9 and 7.9−6.9 (overlapping m, aryl), 4.10, 4.08 and 4.06 (CH_3O); ^{13}C NMR ($CDCl_3$) δ 171.82, 171.69 and 171.23 (acid C=O), 168.39, 168.12 and 163.29 (ester C=O), 163.23, 163.02 and 162.72 (anhydride C=O) [multitude of aromatic peaks of the various isomers deleted] 53.47, 53.41, 53.34 and 53.29 (CH_3O); FTIR (KBr, %T) 3453 (br, 25), 1843 (C=O, 21), 1768 (C=O, 33), 1729 (10), 1444 (35), 1260 (20), 1197 (13), 1176 (33), 1166 (34), 1154 (36), 912 (36), 798 (38), 766 (36) cm^{-1}; MS (EI) *m/e* 418 (6.29), 346 (39.26), 274 (100), 272 (36.95).

Crystallographic Analysis. Crystals of HLDA were grown from slow concentration of a NMP solution. A yellow crystal measuring 0.4 × 0.4 × 0.4 was mounted on a glass fiber and aligned on a Syntex $P2_1$ diffractometer. Final unit cell parameters were determined by least square refinements of 25 reflections with 20° < 2θ < 30°. Crystal data, data collection and reduction, and structure refinement details are listed in Table 2. Crystal stability was monitored by measuring three standard reflections every 97 measurements. Data were corrected for Lorentz and polarization factors and reduced to unscaled F values. Crystallographic calculations were performed by using the Siemens SHELXTYLPLUS (PC Version)[36] program library. The position of all the atoms were determined by direct methods. All non-hydrogen atoms were refined anisotropically by use of full matrix least-squares methods. The hydrogen atoms were refined isotropically with the isotropic thermal parameters fixed at 0.05 Å^2. The final agreement factors for the 1311 data ($F > 2.0\sigma(F)$) were R_f = 3.29, R_{wf} = 3.96, and GOF = 1.11.

Table 2. Crystallographic Data for HLDA

emp form	$C_{52}H_{20}O_{12}$
color; habit	yellow, cubes
form wt	836.7
cryst syst	monoclinic
space grp	*Cc*
cryst size (mm)	0.4 × 0.4 × 0.4
cell constants	
a (Å)	15.860 (3)
b (Å)	9.098 (2)
c, (Å)	12.228 (2)
β (deg)	101.05 (3)
V (Å)^3	1731.8 (6)
Z	2
density (calcd) (g/cm^3)	1.604
absorp. coeff. (mm^{-1})	0.108
F(000)	856
temperature (K)	131
2θ range	3.5 to 45.0°
scan type	ω
scan speed (deg/min)	8.00
scan range (deg)	0.80(w)
no. of reflns collcd	1498
no. of indep reflns	1311
R_{int}%	0.95
no. obsd refl, $F > 2\sigma(F)$	1115
$R(F)$%	3.29
$R_w(F)$%	3.96
GOF	1.11

Acknowledgment. A.A.F. would like to acknowledge the kind and generous support of the National Research Council and NASA Lewis Research Center, in particular the warm hospitality of the Polymers Branch.

JO941976V

(32) Sargent, M. V.; Timmons, C. J. *J. Chem. Soc.* **1964**, Suppl. 1, 5544−5552.
(33) Matsuo, T.; Tanoue, Y.; Matsunaga, T. Nagatoshi, K. *Chem. Lett.* **1972**, 709−712.
(34) Hacker, N. P.; McOmie, J. F. W. *Tetrahedron* **1984**, *40*, 5249−5254.
(35) Hacker, N. P.; McOmie, J. F. W.; Meunir-Piret, J.; Van Meerssche, M. *J. Chem. Soc., Perkin Trans 1* **1982**, 19−23.
(36) Nicolet Instrument Corp., Madison, WI, 1988.

Organometallics **1996**, *15*, 460−463

Preparation and Structural Characterization of a Platinum Catecholate Complex Containing Two 3-Ethynylthiophene Groups

James D. Kinder*

NASA Lewis Research Center, Cleveland, Ohio 44135

Wiley J. Youngs

Department of Chemistry, The University of Akron, Akron, Ohio 44325

Received February 27, 1995®

Summary: The reaction of 1,2-bis(tert-butyldimethylsiloxy)-3,4-bis(3-ethynylthiophene-yl)benzene (4) with Pt(P(Ph)$_3$)$_2$Cl$_2$ and tetrabutylammonium fluoride produces a novel platinum catecholate complex.

The catechol group can coordinate to a variety of transition and main group metals in a wide range of oxidation states.[1] Catechols and metal catecholates have been intensively studied for their unique structural,[2] electronic,[3] magnetic,[4] and catalytic activity.[5] The incorporation of metal catecholates into a conducting polymer matrix provides the opportunity for the construction of modified electrodes that may have interesting electrocatalytic behavior. In this paper, the synthesis, characterization, and electrochemical properties of a platinum catecholate complex containing two 3-ethynylthiophene groups are described.

The synthesis of the platinum catecholate complex **5** is illustrated in Scheme 1. The synthesis of **1** was accomplished by the procedure developed by Kajigaeshi and co-workers.[6] Treatment of **1** with BBr_3 in acetic acid produced the diiodocatechol **2** (94% yield). To prevent the catechol group from complexing the palladium catalyst used in the alkyne coupling reaction, the catechol was protected by reacting **2** with *tert*-butyldimethylsilyl chloride to form **3** (69% yield). The *tert*-butyldimethylsilyl group was chosen due to its

Scheme 1

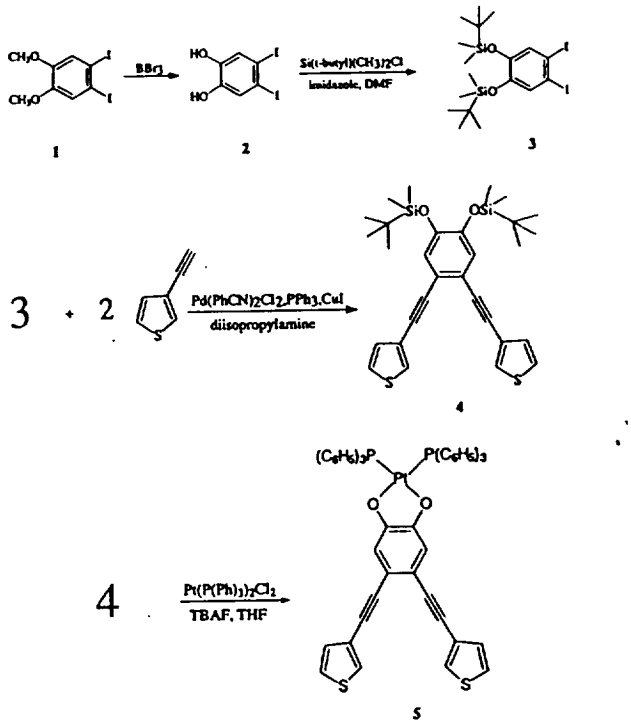

reported stability to a variety of reaction conditions and its facile removal by fluoride ion.[7] Reaction of **3** with 2 equiv of 3-ethynylthiophene[8] in the presence of a palladium catalyst produced the disubstituted product **4** (62% yield).

The formation of metal catecholates normally proceeds by treating a catechol with strong base (e.g., KOH) in the presence of a metal dichloride. However, the platinum catecholate complex **5** formed in high yield (94%) by combining **4** with a THF solution of tetra-*n*-butylammonium fluoride and $Pt(PPh_3)_2Cl_2$. Thus, it was unnecessary to deprotect **4** to form the catechol before reaction with the metal dichloride. The infrared spectrum of **5** showed an intense absorption at 1284 cm^{-1}, indicating a C−O stretching vibration, which is indicative of a metal catecholate structure. The thermal stability of **5** was examined with thermal gravimetric analysis (TGA). A 5% weight loss was observed for **5** at 307 °C in N_2.

• Abstract published in *Advance ACS Abstracts*, October 15, 1995.

(1) (a) Pierpont, C. G.; Buchanan, R. M. *Coord. Chem. Rev.* **1981**, *38*, 45. (b) Blatchford, T. P.; Chisholm, M. H.; Huffman, J. C. *Inorg. Chem.* **1988**, *27*, 2059. (c) Kaim, W. *Coord. Chem. Rev.* **1987**, *76*, 187.

(2) (a) Churchill, M. R.; Lake, C. H.; Paw, W.; Keister, J. B. *Organometallics* **1994**, *13*, 8. (b) Zirong, D.; Bhattacharya, S.; McCusker, J. K.; Hagen, P. M.; Hendrickson, D. N.; Pierpont, C. G. *Inorg. Chem.* **1992**, *31*, 870. (c) Karpishin, T. B.; Stack, T. D. P.; Raymond, K. N. *J. Am. Chem. Soc.* **1993**, *115*, 182.

(3) (a) Bhattacharya, S.; Pierpont, C. *Inorg. Chem.* **1992**, *31*, 35. (b) Dilworth, J. R.; Ibrahim, S. K.; Khan, S. R.; Hursthouse, M. B.; Karaulov, A. *Polyhedron* **1990**, *9*, 1323. (c) Lever, A. B. P.; Auburn, P. R.; Dodsworth, E. S.; Haga, M.; Liu, W.; Melnik, M.; Nevin, W. A. *J. Am. Chem. Soc.* **1988**, *110*, 8076. (d) Bhattacharya, S.; Boone, S. R.; Fox, G. A.; Pierpont, C. *J. Am. Chem. Soc.* **1990**, *112*, 1088.

(4) (a) Coucouvanis, D.; Jonasdottir, S. G.; Christodoulou, D.; Kim, C. G.; Kampf, J. W. *Inorg. Chem.* **1993**, *32*, 2987. (b) Gojon, E.; Latour, J.; Greaves, S. J.; Povey, D. C.; Ramdas, V.; Smith, G. W. *J. Chem. Soc., Dalton Trans.* **1990**, 2043.

(5) (a) Haga, M. *Inorg. Chem.* **1986**, *25*, 447. (b) Persson, C.; Andersson, C. *Polyhedron* **1993**, *12*, 2569. (c) Takacs, J.; Kiprof, P.; Riede, J.; Herrmann, W. *Organometallics* **1990**, *9*, 782. (d) Ueda, C.; Tse, D. C.; Kuwana, T. *Anal. Chem.* **1982**, *54*, 850. (e) Jaegfeldt, H.; Torstensson, A. B. C.; Gorton, L. G. O.; Johansson, G. *Anal. Chem.* **1981**, *53*, 1979. (f) Barbaro, P.; Bianchini, C.; Linn, K.; Mealli, C.; Meli, A.; Vizza, F.; Laschi, F.; Zanello, P. *Inorg. Chim. Acta* **1992**, *198*−*200*, 31.

(6) Kajigaeshi, S.; Kakinami, T.; Moriwaki, M.; Watanabe, M.;

(7) (a) Corey, E. J.; Venkateswarlu, A. *J. Am. Chem. Soc.* **1972**, *94*, 6190. (b) Core, E. J.; Jones, G. B. *J. Org. Chem.* **1992**, *57*, 1028. (c) Corey, E. J.; Yi, K. Y. *Tetrahedron Lett.* **1992**, *33*, 2289.

(8) Youngs, W. J.; Solooki, D.; Tessier, C. A. *Synlett* **1990**, 427.

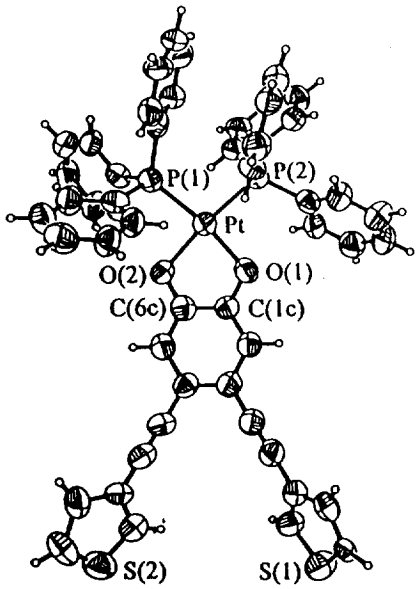

Figure 1. Thermal ellipsoid of 5 drawn at 50% probability. Selected bond distances (Å) and angles (deg): Pt–O(1), 2.028 (8); Pt–O(2), 2.052(9); C(6c)–O(2), 1.333(16); C(1c)–O(1), 1.348(15); P(1)–Pt–O(2), 87.9(3); P(2)–Pt–O(1), 90.5-(3); P(2)–Pt–P(1), 98.6(1).

Crystals of 5 were grown by slow concentration of 5 in methylene chloride. The crystal structure of 5, showing the thermal ellipsoids, is shown in Figure 1. A molecule of methylene chloride is also present in the asymmetric unit. Crystals of 5 were air stable. However, the crystals slowly lost solvent over time, which degraded the quality of the crystals. The geometry of the ligands around the platinum atom is square planar. The thiophene ring containing sulfur atom S1 is twisted (57.7°), and the thiophene ring containing sulfur atom S2 is twisted (29.6°) out of the plane defined by the platinum catecholate structure. The Pt–O bond distances of 2.028(8) and 2.052(9) Å and the C–O bond distances of 1.348(15) and 1.333(16) Å are typical for metal catecholate complexes.

Many thiophene systems can be anodically electropolymerized to form electrically conducting polymers with conductivities as high as 10^2 $(\Omega \cdot cm)^{-1}$. Substituents in the β position on the thiophene ring have a strong influence on both the conductivity and the extent of polymerization of the thiophene monomers. Roncali and co-workers found that when a bulky substituent such as an isopropyl group is attached to the β position on the thiophene ring polymerization can be prevented. By adding two (CH_2) units as spacers between the thiophene and isopropyl groups, polymerization occurred.[9]

The cyclic voltammetry of 5 in 0.1 M TBAP–CH_2Cl_2 is shown in Figure 2. Two one-electron reversible (ΔE = 82 mV, i_a/i_c = 1) oxidation waves at 0.266 and 0.870 V [vs Ag/Ag^+ (CH_3CN)] were observed. Attempts at electropolymerization of 5 failed in CH_2Cl_2 and in a mixture of 1:1 CH_2Cl_2–nitrobenzene. This may be due to steric effects around the thiophene rings. Future work will concentrate on synthesizing new metal catecholate complexes analogous to 5 and examining the electrochemical and optical properties of these new systems.

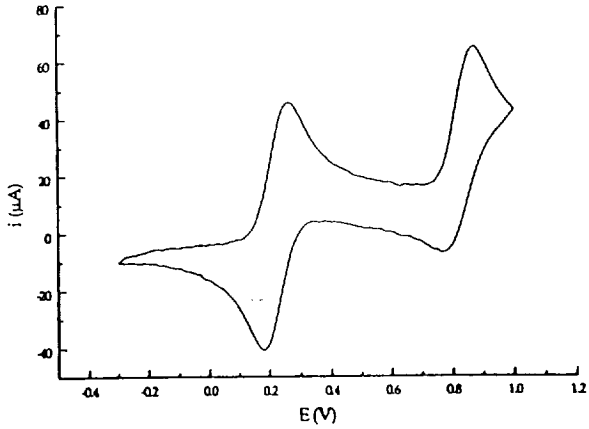

Figure 2. Cyclic voltammogram of 5 (1 mM) in 0.1 M TBAP–CH_2Cl_2. Scan rate was 100 mV s^{-1}.

Experimental Section

Materials. All manipulations were performed using standard inert atmosphere techniques[10] unless otherwise specified. Literature procedures were used to prepare 4,5-diiodoveratrole,[6] 3-ethynylthiophene,[8] and dichlorobis(benzonitrile)palladium(II).[11] Diisopropylamine was distilled from BaO, CH_2Cl_2 from CaH_2, and tetrahydrofuran (THF) from sodium–benzophenone ketyl. Tetrabutylammonium perchlorate (TBAP, Kodak) was recrystallized twice from ethyl acetate–pentane and dried for 48 h at 100 °C (10^{-3} Torr) before use.

Apparatus. NMR spectra were recorded on either a Bruker AC200 or AM300 spectrometer. X-ray diffraction data were collected on a Syntex $P2_1$ single-crystal diffractometer. IR data were collected on a Nicolet 510P FT-IR spectrometer. An EG&G Princeton Applied Research Model 273A potentiostat/galvanostat controlled by the EG&G Princeton Applied Research Model 270 software package was used to monitor the electrochemical measurements. Mass spectra were recorded on a Kratos MS25RFA mass spectrometer. Thermogravimetric analysis was collected on a Perkin-Elmer TGS2-II thermal gravimetric analyzer.

Synthesis of 4,5-Diiodocatechol (2). 4,5-Diiodoveratrole (10.074 g, 26 mmol) was dissolved in $CHCl_3$ and cooled to −60 °C. BBr_3 (9.72 mL, 103 mmol) was slowly added via syringe. After warming to room temperature the mixture was allowed to stir for 6 h and was then poured into ice water. The product was extracted with ether and dried with $MgSO_4$. Evaporation of the solvent produced 8.75 g (94% yield) of 2 as a white powder. ^1H NMR (acetone-d_6, 200 MHz): δ 8.41, 7.35. ^{13}C NMR (acetone-d_6, 300 MHz): δ 147.47, 126.50, 94.50. FT-IR (KBr): 3245(s), 3048(m), 1595(m), 1477(s), 1408(s), 1307(m), 1224(s), 870(s), 701(s) cm^{-1}. HRMS calcd 361.8300, obsd 361.8294.

Synthesis of 1,2-Bis(*tert*-butyldimethylsilyloxy)-4,5-diiodobenzene (3). A solution of imidazole (8.411 g, 124 mmol) and *tert*-butyldimethylsilyl chloride (9.32 g, 62 mmol) dissolved in 50 mL of DMF was added via cannula to 11.193 g (31 mmol) of 4,5-diidocatechol dissolved in 100 mL of DMF. After stirring for 48 h the mixture was poured into water, extracted with ether, and dried with $MgSO_4$. Evaporation of the solvent followed by column chromatography on silica gel eluting with hexane produced 12.54 g (69% yield) of 3 as a white powder. ^1H NMR (acetone-d_6, 200 MHz): δ 7.38, 0.99, 0.23. ^{13}C NMR (acetone-d_6, 300 MHz): δ 148.86, 132.15, 97.14, 26.29, 19.12, −3.94. FT-IR (neat): 2955(s), 2930(s), 2858(s), 1564(w), 1542(m), 1472(s), 1390(m), 1338(s), 1292(s), 1255(s), 1005(w), 932(s) cm^{-1}. HRMS calcd 590.0030, obsd 590.0027.

(9) (a) Roncali, J.; Garreau, R.; Yassar, A.; Marque, P.; Garnier, F.; Lemaire, M. *J. Phys. Chem.* **1987**, *91*, 6706. (b) Roncali, J.; Garreau, R.; Delabouglise, D.; Garnier, F.; Lemaire, M. *Synth. Mett.* **1989**, *28*, C341.

(10) Shriver, D. F. *The Manipulation of Air Sensitive Compounds*; R. E. Krieger Publishing Co.: Malabar, FL, 1982.

(11) Hartly, F. R. *Organomet. Chem. Rev. A* **1970**, *6*, 119.

Table 1. Crystallographic Data for 5

formula	$C_{55}H_{40}Cl_2O_2P_2PtS_2$
formula wt	1124.9
space group	$P2_1/c$
crystal system	monoclinic
cell constants	
a (Å)	18.556(4)
b (Å)	13.562(3)
c (Å)	20.524(4)
β (deg)	110.69(3)
V (Å^3)	4832(2)
Z	4
D (calcd) (g cm^{-3})	1.546
absorp coeff (mm^{-1})	3.221
F(000)	2240.00
temp (K)	133
2θ range (deg)	3.5−45.0
scan type	ω
scan speed (deg/min in ω)	8.72
scan range (ω) (deg)	1.80
no. of reflns collcd	4976
no. of indep reflns	3984 (R_{int} = 2.74%)
refinement method	full-matrix least-squares
no. of obsd reflns	3362 ($F > 4.0\sigma(F)$)
no. of params refined	578
$R(F)$ (%)	5.86
$R_w(F)$ (%)	7.33
GOF	1.14

Synthesis of 1,2-Bis(*tert*-butyldimethylsilyloxy)-4,5-bis(3-ethynylthiophene-yl)benzene (4). Diisopropylamine (150 mL) was added to 0.4547 g (1.2 mmol) of $Pd(Cl)_2(PhCN)_2$, 0.6224 g (2.4 mmol) of PPh_3, 0.1142 g (0.6 mmol) of CuI, and 7.0 g (12 mmol) of **3**. To this solution was added 2.8 g (26 mmol) of 3-ethynylthiophene slowly via syringe. The mixture was heated to 60 °C for 1 h and then cooled to room temperature and stirred for 11 h. The mixture was filtered and the solvent was evaporated. Chromatography on silica gel eluting with a 1:9 CH_2Cl_2−hexane mixture produced 4.0465 g (62% yield) of **4** as a yellow powder. ^{1}H NMR (acetone-d_6, 300 MHz): δ 7.70 (dd, 1 H), 7.53 (dd, 1 H), 7.21 (dd, 1 H), 7.05 (s, 1 H), 1.02 (s, 9 H), 0.28 (s, 3 H). ^{13}C NMR (acetone-d_6, 300 MHz): 148.42, 130.57, 129.63, 127.00, 123.29, 120.40, 88.22, 26.22, 26.37, 19.15, −3.74. FT-IR (KBr): 3106(w), 2954(s), 2930(s), 2858(s), 1594(w), 1529(s), 1494(s), 1492(s), 1362(w), 1331(s), 1255(s), 932(s), 838(s), 781(s) cm^{-1}. HRMS calcd 550.1852, obsd 550.1840.

Synthesis of [4,5-Bis(3-ethynylthiophene-yl)-1,2-benzenediolato(2−)-*O,O'*]bis(triphenylphosphine)platinum-(II) (5). THF (20 mL) was added to a flask containing 1.001 g (1.8 mmol) of **4** and 1.437 g (1.8 mmol) of $Pt(P(Ph)_3)_2Cl_2$. A sample of 7.2 mL of a 1 M tetrabutylammonium fluoride−THF solution was added via syringe. The mixture was allowed to stir for 48 h. After filtration the solvent was removed and the oily residue was washed with hexane. The compound was recrystallized from CH_2Cl_2 to produce 1.758 g (94% yield) of **5** as yellow crystals. ^{1}H NMR ($CDCl_3$, 300 MHz): δ 7.58−7.06 (m), 6.54 (s). ^{13}C NMR ($CDCl_3$, 300 MHz): δ 164.43, 134.77 (dd), 130.79, 130.11, 128.76 (dd), 127.94 (dd), 126.43, 124.54, 124.08, 117.93, 113.46, 90.63, 84.16. FT-IR (KBr): 2203(w), 1483(m), 1437(s), 1284(s), 1231(s), 1098(s), 781(m) cm^{-1}. Anal. Calcd for $C_{55}H_{40}O_2P_2PtS_2Cl_2$: C, 58.72; H, 3.58; S, 5.70. Found: C, 59.16; H, 4.00; S, 5.70.

Electrochemical Measurements. A three-compartment electrochemical cell (~25 mL capacity) was used for electrochemical measurements. A coiled Pt wire was used as a counter electrode and separated from the working electrode compartment by a glass frit. The reference electrode was Ag/Ag$^+$ (CH_3CN, 0.1 M TBAP). The working electrode was a platinum disk (diameter = 5 mm). The concentration of **5** was 1.0×10^{-3} M in 0.10 M TBAP−CH_2Cl_2.

X-ray Crystallographic Data for 5. Crystals of **5** were grown by slow concentration of a CH_2Cl_2 solution. A yellow crystal measuring 0.4 × 0.4 × 0.4 was mounted on a glass fiber and aligned on the diffractometer. Final unit cell parameters were determined by least-squares refinement of 25 reflection with $20° < 2\theta < 30°$. Crystal data, data collection and reduction, and structure refinement details are listed in Table 1. Crystal stability was monitored by measuring three

Table 2. Atomic Coordinates ($\times 10^5$) and Equivalent Isotropic Displacement Coefficients (Å^2 × 10^4)

	x	y	z	U(eq)[a]
Pt(1)	20807(3)	9618(4)	7994(3)	630(3)
P(2)	18558(20)	6912(27)	−3323(18)	666(15)
P(1)	18123(21)	25779(26)	7434(17)	665(14)
O(2)	23500(50)	10499(61)	18575(45)	686(38)
C(5B)	18993(83)	−22866(116)	−4173(72)	803(69)
O(1)	24250(48)	−4567(63)	10237(44)	681(38)
C(1D)	8411(70)	6961(87)	−9074(65)	583(55)
C(2I)	42223(73)	−10296(107)	52647(74)	703(66)
C(3)	39736(85)	−9300(100)	45314(101)	807(81)
C(2D)	6547(85)	4222(95)	−15897(72)	741(68)
C(2H)	47971(82)	−39381(102)	35427(71)	742(65)
C(5A)	22215(85)	43799(109)	−6851(74)	785(69)
C(5D)	−5006(84)	7916(98)	−10702(79)	731(69)
C(1A)	16986(70)	32929(85)	−394(67)	586(57)
C(6B)	1771(79)	−13208(113)	−2932(66)	711(64)
C(2A)	10315(73)	32213(96)	−6114(68)	659(58)
C(2)	39458(89)	−23829(125)	30134(75)	736(68)
C(1I)	42642(88)	−18993(130)	56104(82)	976(78)
C(6A)	22941(88)	38662(103)	−740(80)	776(68)
C(3C)	35046(74)	−15415(107)	27267(73)	709(65)
C(6E)	7302(80)	22282(115)	13561(75)	812(66)
C(3A)	9512(86)	37239(105)	−12243(77)	752(67)
C(4C)	34203(73)	−7900(103)	31521(74)	678(65)
C(1H)	46397(75)	−45476(108)	40175(72)	775(62)
C(4)	37378(78)	−8521(98)	39107(89)	728(70)
C(2E)	5670(85)	37679(104)	7619(75)	761(66)
C(4B)	24268(83)	−24697(109)	−7379(75)	798(67)
C(3I)	44660(97)	−2630(124)	57513(82)	1020(81)
C(2B)	26387(81)	−7682(107)	−7942(74)	736(67)
C(6D)	2758(86)	8665(86)	−6264(72)	703(65)
C(1E)	9523(69)	28727(112)	9520(64)	668(56)
C(1C)	27508(67)	−5696(98)	17191(69)	609(60)
C(4D)	−6863(82)	5477(110)	−17469(82)	791(70)
C(3D)	−1222(82)	3414(106)	−20059(71)	783(66)
C(6C)	26941(70)	2131(111)	21446(71)	665(65)
C(1)	43548(94)	−30578(121)	32372(75)	800(70)
C(1B)	21253(76)	−5629(97)	−4905(62)	626(54)
C(5C)	30215(70)	963(104)	28542(73)	699(63)
C(2C)	31401(72)	−14224(97)	19962(71)	658(60)
C(3B)	28080(80)	−17232(123)	−9207(78)	850(72)
C(4A)	15428(84)	42824(100)	−12644(67)	688(62)
C(3H)	54595(76)	−42910(105)	34116(67)	723(61)
C(2F)	32002(74)	15851(97)	−2541(66)	660(57)
C(1G)	26041(82)	31903(105)	14101(67)	745(66)
C(6F)	21702(78)	18666(88)	−13370(72)	654(60)
C(3F)	36895(84)	21037(117)	−5024(83)	831(70)
C(2G)	24963(91)	39716(107)	18209(82)	801(70)
C(5F)	26944(90)	23582(102)	−15782(78)	777(68)
C(5E)	1125(85)	24549(1109)	15668(81)	824(72)
C(1F)	24317(75)	14644(91)	−6963(67)	627(61)
C(6G)	33495(83)	28844(102)	15447(70)	740(63)
C(5G)	39689(82)	32987(107)	20255(81)	789(66)
C(4G)	38662(100)	40770(134)	23987(87)	940(82)
C(4F)	34310(93)	24835(96)	−11695(83)	757(74)
C(3G)	31087(121)	43925(122)	23052(81)	1001(88)
C(5)	17019(98)	67725(151)	16913(166)	1993(199)
Cl	13095(46)	63465(77)	23209(37)	2015(45)
Cl(1)	10944(37)	65283(45)	8784(33)	1442(32)
C(3E)	−127(98)	40034(113)	9968(85)	884(75)
C(4E)	−2757(90)	33500(122)	13708(78)	859(73)
S(1)	52702(25)	−54664(34)	42833(24)	1010(21)
S(2)	45603(41)	−17690(58)	64545(33)	1090(33)
C(4I)	47290(57)	−6691(85)	65163(45)	1107(50)
C(4H)	57854(58)	−52023(100)	38115(54)	585(50)

[a] Equivalent isotropic U is defined as one-third of the trace of the orthogonalized U_{ij} tensor.

standard reflections every 97 measurements. Data were corrected for Lorentz and polarization factors and reduced to unscaled F values. Crystallographic calculations were performed by using the Siemens SHELXTYLPLUS (PC version)[12] program library. The positions of all non-hydrogen atoms were determined by direct methods. Hydrogen atoms were included using a riding model with $d(C-H) = 0.95$ Å, and the isotropic thermal parameters were fixed at 0.08 Å^2. A disorder model for sulfur atom S2 and carbon atom C4I was used. The final agreement factors for the 3362 data ($|F_o| > 4.0\sigma(|F_o|)$) were $R_f = 5.86$ and $R_{wf} = 7.33$ and GOF = 1.14.

(12) Nicolet Instrument Corp., Madison, WI, 1988.

Supporting Information Available: Tables of atomic coordinates, bond lengths and angles, and anisotropic displacement coefficients (17 pages). Ordering information is given on any current masthead page.

OM950155T

Rigid-Rod Polyimides Based on Noncoplanar 4,4′-Biphenyldiamines: A Review of Polymer Properties vs Configuration of Diamines

Kathy C. Chuang,*,† James D. Kinder,†,‡ Diana L. Hull,§ David B. McConville,§ and Wiley J. Youngs§

NASA Lewis Research Center, Cleveland, Ohio 44135, and Department of Chemistry, University of Akron, Akron, Ohio 44325

Received March 6, 1997; Revised Manuscript Received July 14, 1997•

ABSTRACT: X-ray crystal structures of three substituted 4,4′-biphenyldiamines, namely, 2,2′,6,6′-tetramethylbenzidine (TMBZ), 2,2′-dimethylbenzidine (DMBZ) and 2,2′-bis(trifluoromethyl)benzidine (BFBZ), were determined. The torsional angles between the two phenyl rings for TMBZ, DMBZ, and BFBZ are $\phi = 83°$, 75°, and 59°, respectively. A structure–property relationship between the three-dimensional configuration of diamine monomers and the corresponding polyimides is discussed.

Introduction

Rigid-rod polymers such as Kevlar[1] and poly(benzobis-(oxazole)),[2] are well-known for their interesting liquid crystalline behavior[3,4] and outstanding performance as high-strength, high-modulus fibers. However, rigid-rod polymers are often insoluble in common organic solvents and difficult to process. Efforts to increase the solubility of rodlike polymers have included the use of bulky substituents, kinks, crank-shaft, and noncoplanar biphenyl moieties.[5–7] Previously, polyamides[8] and polyimides containing 2,2′-substituted 4,4′-biphenyldiamine (i.e., 2,2′-substituted benzidine) have been shown to display optical transparency and improved solubility. The substitution at the 2- and 2′-positions of the biphenyl moiety appears to force the two phenyl rings into adopting a noncoplanar conformation. This, in turn, disrupts the crystal packing and provides enhanced solubility. Recently, considerable efforts in molecular modeling have been devoted to calculating the torsional angle between the two phenyl rings on either the 2,2′-substituted biphenyl[9,10] or the polyimide copolymers[11] based on 2,2′-substituted benzidines. However, to the best of our knowledge, no X-ray structure has ever been published on the noncoplanar, substituted benzidine derivatives. The purpose of this research is to investigate the correlation between physical properties of polyimides and three-dimensional structures of the corresponding diamine monomers, i.e., noncoplanar, substituted benzidines. Property–structure relationships, such as glass transition temperature (T_g) and solubility of polyimides *versus* X-ray crystal structures of the corresponding substituted benzidines, will be explored. Hopefully, information about the torsional angle between the two phenyl rings and the placement of the substituents on benzidine will provide some insights complementary to the results of molecular modeling on these polymers.

Thermoplastic polyimides, prepared from 2,2′-dimethylbenzidine, 2,2′-bis(trifluoromethyl)benzidine, and 2,2′,6,6′-tetramethylbenzidine with various aromatic dianhydrides in a high boiling solvent, such as *m*-cresol, had high molecular weight and could be spun into high-strength, high-modulus fibers.[12] Furthermore, these polyimides also exhibited excellent thermal stability, low coefficients of thermal expansion (CTE) and low dielectric constants, suitable for electronic packaging.[13–15] Thermosetting polyimides derived from 4,4′-(hexafluoroisopropyliene)diphthalic anhydride (HFDA) and 2,2′,6,6′-tetramethylbenzidine exhibited higher T_g's than the corresponding polyimides containing 2,2′-bis(trifluoromethyl)benzidine.[16,17] This article will relate the properties of thermoplastic polyimides, derived from 2,2′-dimethylbenzidine (DMBZ), 2,2′-bis(trifluoromethyl) benzidine (BFBZ), and 2,2′,6,6′-tetramethylbenzidine (TMBZ), to the X-ray crystal structures of these three substituted benzidines.

Experimental Section

Materials. All the dianhydrides, 2,2′-bis(trifluoromethyl)-benzidine, and 2,2′-dimethylbenzidine (i.e., *m*-tolidine, received as dihydrochlorides) used in this study were purchased from Chriskev Co., Inc. The dianhydrides were dried at 150 °C under vacuum prior to use. 2,2′,6,6′-Tetramethylbenzidine was synthesized following a reported procedure.[17] The *m*-cresol, obtained from Aldrich Chemical Co., was distilled from phosphorus pentaoxide under vacuum.

Polymer Synthesis and Sample Preparation. The polymerization[18] (Figure 1) was accomplished by reacting a dianhydride, such as 3,3′,4,4′-biphenyltetracarboxylic dianhydride (BPDA), with a selected 4,4′-biphenyldiamine (either TMBZ, DMBZ, or BFBZ) in *m*-cresol overnight at room temperature to form the poly(amic acid). Isoquinoline (1 wt %) was added initially as a catalyst. The poly(amic acid) was then heated to reflux for 6 h to afford the corresponding polyimides. However, certain polyimides precipitated out prematurely, depending on the substituted benzidine used in the polymerization. No further characterization was attempted on these precipitated polyimides. The TMBZ–BPDA and BFBZ–BPDA fibers were produced from an isotropic solution of 10% (w/w) polyimides in *m*-cresol, via a dry-jet wet spinning process into a coagulation bath of water/acetone.[19] The as-spun fibers, which had little tensile strength, were then drawn at an elevated temperature (>400 °C) up to 6 to 10 times draw ratio in air by a zone drawing method. An exception, DMBZ–BPDA was polymerized and spun from *p*-chlorophenol as reported in the literature.[20] The single crystals of TMBZ, DMBZ, and BFBZ were obtained by recrystallization from benzene and petroleum ether.

X-ray Crystallography. Crystallographic data for the three substituted benzidines (TMBZ, DMBZ, BFBZ) were

* To whom corespondence should be addressed.
† NASA Lewis Research Center.
‡ Postdoctor fellow of National Research Council (1992–1995). Present address: Ferro Corp., Cleveland, OH 44131.
§ University of Akron.
• Abstract published in *Advance ACS Abstracts*, October 15, 1997.

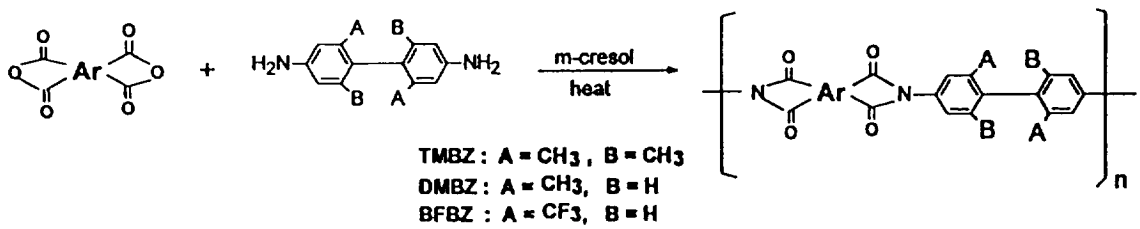

Figure 1. Polyimide synthesis.

collected at low temperature using a Syntex $P2_1$ diffractometer employing Mo Kα radiation (λ = 0.710 71 Å). Intensity data for each were collected between 3.5° and 50.0° in 2θ using the ω scan technique at 8.37 deg/min^{-1} with a scan range of 2.00°. TMBZ ($C_{16}H_{20}N_{22}$, white parellpiped) formed in monoclinic space group $P2_1/c$ with 13 formula units per unit cell: a = 11.366(2) Å, b = 16.533(3) Å, c = 22.424(4) Å, $\alpha = \gamma = 90°$, β = 100.05(3)°, V = 4149.2(1) Å^3, density (calculated) = 1.154 Mg/m^3, as determined from reflections in the 2θ range of 3.5° to 45.0° at 105 K. The asymmetric unit cell contained three independent molecules. DMBZ ($C_{14}H_{16}N_2$) crystallized in the orthorhombic space group *Pbca* (#61) with 8 formula units per unit cell: a = 14.580(3) Å, b = 7.502(3) Å, c = 21.133(5) Å, $\alpha = \beta = \gamma = 90°$, V = 2311.4(1) Å^3, density (calculated) = 1.220 Mg/m^3, determined from 25 reflections in the 2θ range of 20° to 30° at 157 K. BFBZ ($C_{14}H_{10}N_2F_6$) solved in the orthorhombic space group *Pbcn* (#60) with 4 formula units per unit cell: a = 12.937(3) Å, b = 5.847(1) Å, c = 17.649(4) Å, $\alpha = \beta = \gamma$ = 90°, V = 1334.9(5) Å^3, density (calculated) = 1.593 Mg/m^3, as deduced from 29 reflections in the 2θ range of 20° to 30° at 139 K. All the structures were solved by direct methods using the SHELXTL PLUS program set.[24] All non-hydrogen atoms were located from the initial E-maps and refined by full-matrix least squares on F^2 using the program SHELXL-93.[25] Corrections for the effects of primary and secondary extinction were applied (extinction coefficient = 0.0006(2) for TMBZ, 0.019(2) for DMBZ, and 0.010(2) for BFBZ).[26] All hydrogen atoms, with the exception of those of the amino groups, were placed in idealized positions and refined using a riding model. The amino hydrogen atoms were located from the difference-Fourier maps for both compounds. The TMBZ coordinates of amino hydrogen's were refined *via* a riding model. Refinement to convergence of 488 parameters on 3858 unique data (R_{int} = 0.0188) afforded a weighted discrepancy index[27] of 7.98% (R = 6.54% for 3858 data with $F_o^2 > 4\sigma(F_o^2)$),[28] and a goodness-of-fit[29] of 2.14). For DMBZ, refinement to convergence of 160 parameters on 1829 unique data (R_{int} = 0.0169) yielded a weighted R factor[27] of 7.28% (R = 3.43% for 1265 data with $F_o^2 > 4\sigma(F_o^2)$) and a goodness-of-fit of 1.012 for DMBZ. For BFBZ, 101 parameters were refined against 1171 unique data (R_{int} = 0.0277) to produce a weighted R factor of 7.18% (R = 2.98% for 833 data *with* $F_o^2 > 4\sigma(F_o)^2$ and a goodness-of-fit of 1.002).

Inspection of the difference-Fourier maps for DMBZ showed some disorder of the methyl groups. These groups were refined as an ideally disordered rotor in which one part of the disordered group is offset from the other by 60°. The site occupation factor of one part was set equal to a free variable while the site occupancy of the other was set to one minus that free variable. This treatment gave site occupation factor for the primary parts of 71.7% for C(13) and 66.3% for C(14). the isoptropic Uvalues of both parts were set equal to 1.5 times that of the carbon atom. The trifluoromethyl group of BFBZ, however, showed no evidence of rotational disorder with largest U_{eq} value being that of F(2) at 1.7 times the value of C(7).

The phenyl rings in each compound are rotated about the joining sigma (σ) bond. The angle between the least-squares planes as defined by the phenyl ring carbon atoms in TMBZ, DMBZ, and BFBZ are 83°, 75°, and 59°. The structure determination summaries for TMBZ, DMBZ, and BFBZ are listed in Table 1, Table 2, and Table 3, respectively. Other X-ray crystallography information concerning the atomic coordinates and equivalent isotropic displacement coefficients, bond lengths, and bond angles are listed in Tables 4–6 for TMBZ, Tables 7–9 for DMBZ, and Tables 10–12 for BFBZ. Additional X-ray crystallography data such as anisotropic displacement coefficients, H-atom coordinates, and isotropic displacement as well as observed and calculated structure factors are available as Supporting Information.

Results and Discussion

As shown in the X-ray structure, the torsional angle between the two phenyl rings of TMBZ is ϕ = 83° (Figure 2), compared to that of ϕ = 75° for DMBZ (Figure 3) and ϕ = 59° for BFBZ (Figure 4). However, the difference in torsional angle did not seem to have any effect on the chemical shifts (Table 14) of ^{13}C-NMR spectra of TMBZ, DMBZ, and BFBZ (Figure 5) as well

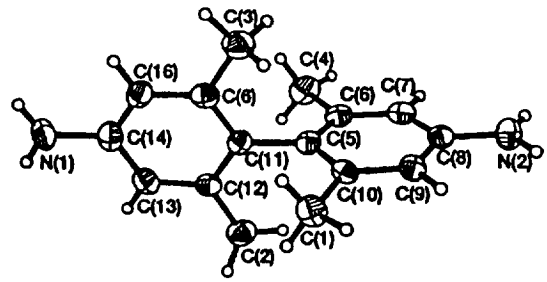

Figure 2. Molecular configuration of 2,2′,6,6′-tetramethylbenzidine (TMBZ).

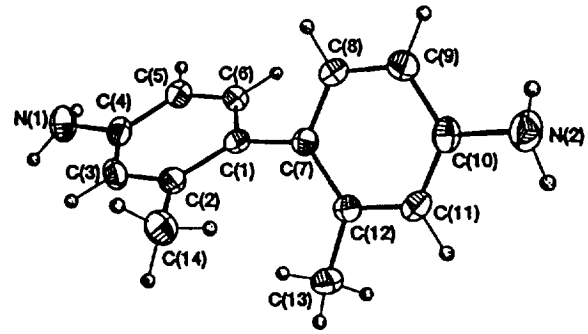

Figure 3. Molecular configuration of 2,2′-dimethylbenzidine (DMBZ).

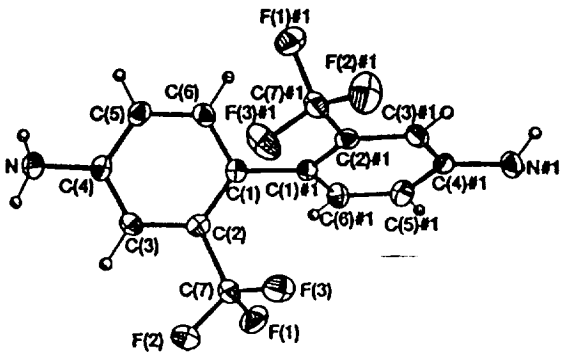

Figure 4. Molecular configuration of 2,2′-bis(trifluoromethyl)-benzidine (BFBZ).

Table 1. Structure Determination Summary for TMBZ

Crystal Data

empirical formula	$C_{16}H_{20}N_2$	unit cell dimensions	$a = 11.366(2)$ Å	volume	4149.2(13) Å^3
color; habit	white parellpiped		$b = 16.533(3)$ Å	Z	13
crystal size (mm)	0.3 × 0.3 × 0.5		$c = 22.424(4)$ Å	formula weight	221.9
crystal	system monoclinic		$\beta = 100.05(3)$ Å	density (calcd)	1.154 Mg/m^3
space group	$P2_1/c$			absorption coefficient	0.064 mm^{-1}
				$F(000)$	1560

Data Collection

diffractometer used	Siemens R3m/V	standard reflections	3 measured every 97 reflections
radiation	Mo Kα ($\lambda = 0.710\ 73$ Å)	index ranges	$-12 \le h \le 0, 0 \le k \le 17, -23 \le l \le 24$
temperature (K)	103	reflections collected	5739
monochromator	highly oriented graphite crystal	independent reflections	5418 ($R_{int} = 1.88\%$)
2θ range	3.5−45.0°	observed reflections	3858 ($F > 4.0\sigma(F)$)
scan type	ω	absorption correction	N/A
scan speed constant	0.50 deg/min in ω		
scan range (ω)	0.50°		
background measurement	stationary crystal and stationary counter at beginning and end of scan, each for 12.5% of total scan time		

Solution and Refinement

system used	SHELXTL PLUS (PC Version)	no. of parameters refined	488
solution	direct methods	final R indices (obsd data)	$R = 6.47\%$, wR = 7.50%
refinement method	full-matrix least squares	R indices (all data)	R 9.26%, wR = 7.88%
quantity minimized	$\Sigma w(F_o - F_c)^2$	goodness-of-fit	2.09
absolute structure	N/A	largest and mean Δ/σ	0.032, 0.006
extinction correction	$\chi = 0.0006\ (2)$, where $F^* = F[1 + 0.002\chi F^2/\sin(2\theta)]^{-1/4}$	data-to-parameter ratio	7.9:1
hydrogen atoms	riding model, fixed isotropic U	largest difference peak	0.48 e Å^{-3}
weighting scheme	$w^{-1} = \sigma^2(F) + 0.0004F^2$	largest difference hole	−0.33 e Å^{-3}

Table 2. Crystal Data and Structure Refinement for DMBZ

empirical formula: $C_{14}H_{16}N_2$
formula weight: 212.29
temperature: 157 K
wavelength: 0.717073 Å
crystal system: orthorhombic
space group: *Pbca*
unit cell dimensions $a = 14.580(3)$ Å, $\alpha = 90°$
$b = 7.502(3)$ Å, $\beta = 90°$
$c = 21.133(5)$ Å, $\gamma = 90°$
volume, Z: 2311.4(10) Å^3, 8
density (calculated): 1.220 Mg/m^3
absorption coefficient: 0.073 mm^{-1}
$F(000)$: 912
crystal size: 0.58 × 0.52 × 0.24 mm

diffractometer used: Syntex $P2_1$
monochromator: highly oriented graphite crystal
scan type: ω
scan range: 2.00°
scan speed: constant; 8.37 deg/min in ω
background measurement: stationary crystal and stationary counter at beginning and end of scan, each for 25% of total scan time

standard reflections: 3 measured every 97 reflections
range for data collection: 1.93 to 24.07°
limiting indices: $-1 \le h \le 16, -1 \le k \le 8, -24 \le l \le 1$
reflections collected: 2442
independent reflections: 1829 [$R_{int} = 0.0169$]

program set: SHELXTL PLUS Version 5γ
structure solution: Direct methods
refinement program: SHELXTL-93 (Sheldrick, G. M. *SHELXL-93 Program for the refinement of crystal structures.* Univ of Gottingen, Germany, 1993)
refinement method: full-matrix least squares on F^2
hydrogen atom location: all H atoms were placed in idealized positions except those of the amino groups which werer located from difference-Fourier maps
hydrogen atom treatment: Hydrogen atoms were refined using a riding model with isotropic U values fixed at 1.2 times (for aryl) and 1.5 times (for amino and methyl) the U_{eq} of the previous normal atom. The methyl groups were modeled as ideally disordered rigid rotors. The site occupancy of one set of hydrogens was set equal to a free variable while the other group was set equal to one minus that free variable. The coordinates of the amino hydrogen atoms were allowed to refine independently of the corresponding nitrogen atoms.
Data/restraints/parameters: 1829/0/160
goodness-of-fit on F^2: 1.012
weighting scheme: $w = 1/[\sigma^2(F_o^2) + (0.0320P)^2 + 0.0000P]$, where $P = (F_o^2 + 2F_c^2)/3$
final R indices [$I > 2\sigma I$]: R1 = 0.0343, wR2 = 0.0704
R indices (all data): R1 = 0.0518, wR2 = 0.0728
extinction coefficient: 0.019(2)
extinction expression: $F_c^* = kF_c\,[1 + 0.001F_c^2\lambda^3/\sin(2\theta)]^{-1/4}$
shift/esd max and mean: 0.000 and 0.000
largest diff peak and hole: 0.173 and −0.142 e Å^{-3}
refinement details: Refinement was performed on F^2 for all reflections. Weighted R-factors, wR2, and all goodnesses of fit, S, are based on F^2, and conventional R-factors, R1, are based on F, with F set to zero for negative F^2. The observed criterion of $I > 2\sigma I$ is used only for calculating the observed R factor and is not relevant to the choice of reflections used in refinement. R-factors based on F^2 are statistically about twice as large as those based on F, and R-factors based on all data will be even larger.

Table 3. Crystal Data and Structure Refinement for BFBZ

empirical formula: $C_{14}H_{10}F_6N_2$
formula weight: 320.24
temperature: 139 K
wavelength: 0.71073 Å (Mo Kα)
crystal system: orthorhombic
unit cell dimensions: $a = 12.937(3)$ Å
$b = 5.8467(14)$ Å
$c = 17.649(4)$ Å
volume, Z: 1334.9(5) Å^3, 4
space group: *Pbcn*
density (calculated): 1.593 Mg/m^3
absorption coefficient: 0.154 mm^{-1}
$F(000)$: 648
crystal size: 0.64 × 0.36 × 0.2 mm

diffractometer used: Syntex $P2_1$
monochromator: Highly oriented graphite crystal
scan type: ω
scan range: 2.00°
scan speed: constant; 8.37°/min in ω
background measurement: stationary crystal and stationary counter at beginning and end of scan, each for 25% of total scan time
standard reflections: 3 measured every 97 reflections
theta range for data collection: 2.31 to 24.98°
limiting indices: $-1 \le h \le 15$, $-1 \le k \le 6$, $-20 \le l \le 1$
reflections collected: 1631
independent reflections: 1171 [$R_{int} = 0.0277$]

program set: SHELXTL PLUS Version 5γ
structure solution: direct methods
refinement program: SHELXTL-93 (Sheldrick, G.M. *SHELXTL-93 Program for the refinement of crystal structures*. Univ of Gottingen, Germany, 1993)
refinement method: full-matrix least squares on F^2
hydrogen atom location: all H atoms were placed in idealized positions except those of the amino group which were located from difference-Fourier maps
hydrogen atom treatment: Aryl hydrogen atoms were refined using a riding model with isotropic U values fixed at 1.2 times the U_{eq} of the previous normal atom. The amino hydrogen atoms were also allowed to ride but the isotropic U values were held fixed.
data/restraints/parameters: 1171/0/101
goodness-of-fit on F^2: 1.002
weighting scheme: $w = 1/[\sigma^2(F_o^2) + (0.0350P)^2 + 0.0000P]$ where $P = (F_o^2 + 2F_c^2)/3$
final R indices [$I > 2\sigma I$)]: R1 = 0.0298, wR2 = 0.0692
R indices (all data): R1 = 0.0476, wR2 = 0.0718
extinction coefficient: 0.010(2)
extinction expression: $F_c^* = kF_c[1 + 0.001F_c^2\lambda^3/\sin(2\theta)]^{-1/4}$
shift/esd max and mean: 0.002 and 0.000
largest diff peak and hole: 0.165 and −0.157 e Å^{-3}
refinement details: Refinement was performed on F^2 for all reflections. Weighted R-factors, wR2, and all goodnesses of fit, S, are based on F^2, and conventional R-factors, R1, are based on F, with F set to zero for negative F^2. The observed criterion of $I > 2\sigma I$ is used only for calculating the observed R factor and is not relevant to the choice of reflections used in refinement. R-factors based on F^2 are statistically about twice as large as those based on F, and R-factors based on all data will be even larger.

Table 4. Atomic Coordinates (×10^5) and Equivalent Isotropic Displacement Coefficients (Å^2 × 10^4) for TMBZ

	x	y	z	U(eq)[a]		x	y	z	U(eq)[a]
N(1)	45 152 (34)	57 615 (26)	−40 545 (17)	464 (16)	C(6A)	−4 099 (37)	52 684 (25)	35 501 (19)	254 (15)
N(2)	58 609 (34)	89 742 (22)	−2 631 (16)	377 (15)	C(7A)	−5 232 (36)	50 185 (26)	24 383 (18)	237 (15)
N(1A)	−24 585 (30)	50 863 (22)	6 576 (15)	327 (14)	C(8A)	−10 527 (38)	43 228 (25)	21 670 (19)	268 (16)
N(2A)	20 891 (34)	52 303 (23)	48 514 (16)	391 (15)	C(9A)	−16 859 (37)	43 492 (26)	15 800 (19)	261 (16)
N(1B)	−55 039 (30)	12 986 (24)	49 303 (17)	398 (15)	C(10A)	−18 033 (35)	50 596 (25)	12 507 (18)	233 (15)
N(2B)	26 554 (30)	27 712 (22)	43 656 (16)	336 (14)	C(11A)	−12 679 (36)	57 530 (25)	15 198 (19)	269 (16)
C(2)	53 537 (37)	74 831 (27)	−30 084 (20)	291 (16)	C(12A)	−6 300 (36)	57 426 (25)	21 075 (19)	240 (15)
C(3)	50 908 (36)	70 227 (29)	−35 365 (21)	327 (17)	C(13A)	20 030 (40)	45 435 (29)	27 015 (20)	382 (18)
C(4)	47 487 (38)	62 169 (30)	−35 168 (21)	339 (18)	C(14A)	−9 608 (48)	35 309 (26)	25 035 (21)	448 (19)
C(5)	46 741 (38)	58 722 (28)	−29 602 (21)	330 (17)	C(15A)	−17 176 (38)	54 662 (29)	34 313 (21)	359 (18)
C(6)	49 067 (38)	63 234 (28)	−24 267 (21)	305 (17)	C(16A)	−685 (40)	65 197 (25)	23 717 (20)	350 (17)
C(7)	54 258 (38)	76 423 (24)	−18 894 (19)	252 (15)	C(1B)	−19 399 (35)	18 201 (24)	48 014 (18)	210 (14)
C(8)	64 991 (37)	76 113 (26)	−14 753 (19)	261 (16)	C(2B)	−26 064 (36)	12 850 (25)	43 910 (18)	232 (15)
C(9)	66 223 (38)	80 566 (26)	−9 418 (19)	284 (16)	C(3B)	−37 731 (37)	10 892 (26)	44 479 (19)	275 (16)
C(10)	57 084 (39)	85 387 (25)	−8 104 (19)	277 (16)	C(4B)	−43 009 (36)	14 406 (26)	49 028 (20)	283 (16)
C(11)	46 584 (38)	85 954 (25)	−12 328 (20)	298 (17)	C(5B)	−36 259 (36)	19 578 (25)	53 128 (19)	251 (15)
C(12)	45 105 (38)	81 542 (26)	−17 653 (20)	286 (16)	C(6B)	−24 538 (35)	21 442 (25)	52 725 (18)	219 (15)
C(13)	57 781 (43)	83 441 (29)	−30 469 (21)	426 (19)	C(7B)	−7 251 (36)	20 757 (25)	47 122 (18)	236 (15)
C(14)	75 428 (38)	71 189 (29)	−16 078 (21)	381 (18)	C(8B)	3 071 (35)	16 870 (25)	50 015 (18)	224 (15)
C(15)	47 787 (44)	59 251 (29)	−18 399 (21)	416 (19)	C(9B)	14 107 (36)	19 307 (25)	48 887 (18)	232 (15)
C(1)	52 428 (35)	71 391 (26)	−24 514 (19)	253 (16)	C(10B)	15 214 (37)	25 476 (26)	44 818 (19)	257 (15)
C(16)	33 430 (38)	82 224 (30)	−22 022 (22)	429 (19)	C(11B)	4 986 (37)	29 599 (26)	42 118 (18)	261 (15)
C(1A)	1 583 (37)	50 225 (23)	30 780 (19)	226 (15)	C(12B)	−6 182 (37)	27 278 (25)	43 224 (18)	241 (15)
C(2A)	13 647 (38)	48 182 (24)	32 034 (19)	250 (16)	C(13B)	−20 924 (39)	9 210 (27)	38 721 (19)	319 (16)
C(3A)	19 993 (39)	48 662 (24)	37 926 (19)	279 (16)	C(14B)	2 372 (39)	10 082 (26)	54 449 (20)	322 (16)
C(4A)	14 360 (40)	51 328 (25)	42 632 (20)	290 (17)	C(15B)	−17 564 (37)	27 172 (26)	57 261 (20)	315 (16)
C(5A)	2 393 (40)	53 271 (26)	41 355 (20)	304 (17)	C(16B)	−17 155 (39)	31 826 (27)	40 271 (20)	354 (17)

[a] Equivalent isotropic U defined as one-third of the trace of the orthogonalized U_{ij} tensor.

Table 5. Bond Length (Å) for TMBZ

N(1)–C(4)	1.407(6)	C(7)–C(8)	1.399(5)	C(4A)–C(5A)	1.378(6)	C(2B)–C(3B)	1.392(6)
N(2)–C(10)	1.407(6)	C(7)–C(12)	1.406(6)	C(5A)–C(6A)	1.392(6)	C(2B)–C(13B)	1.515(6)
N(1A)–C(10A)	1.407(5)	C(7)–C(1)	1.494(6)	C(6A)–C(15A)	1.500(6)	C(3B)–C(4B)	1.397(7)
N(2A)–C(4A)	1.405(5)	C(8)–C(9)	1.391(6)	C(7A)–C(8A)	1.388(6)	C(4B)–C(5B)	1.385(6)
N(1B)–C(4B)	1.399(6)	C(8)–C(14)	1.510(6)	C(7A)–C(12A)	1.402(6)	C(5B)–C(6B)	1.386(6)
N(2B)–C(10B)	1.408(6)	C(9)–C(10)	1.381(6)	C(8A)–C(9A)	1.386(6)	C(6B)–C(15B)	1.510(6)
C(2)–C(3)	1.396(6)	C(10)–C(11)	1.391(6)	C(8A)–C(14A)	1.506(6)	C(7B)–C(8B)	1.394(5)
C(2)–C(13)	1.510(7)	C(11)–C(12)	1.384(6)	C(9A)–C(10A)	1.381(6)	C(7B)–C(12B)	1.407(6)
C(2)–C(1)	1.398(6)	C(12)–C(16)	1.510(6)	C(10A)–C(11A)	1.386(6)	C(8B)–C(9B)	1.382(6)
C(3)–C(4)	1.391(7)	C(1A)–C(2A)	1.392(6)	C(11A)–C(12A)	1.389(6)	C(8B)–C(14B)	1.511(6)
C(4)–C(5)	1.388(7)	C(1A)–C(6A)	1.393(6)	C(12A)–C(16A)	1.509(6)	C(9B)–C(10B)	1.389(6)
C(5)–C(6)	1.395(6)	C(1A)–C(7A)	1.507(5)	C(1B)–C(2B)	1.400(5)	C(10B)–C(11B)	1.392(6)
C(6)–C(15)	1.501(7)	C(2A)–C(3A)	1.393(6)	C(1B)–C(6B)	1.400(6)	C(11B)–C(12B)	1.389(6)
C(6)–C(1)	1.405(6)	C(2A)–C(13A)	1.511(7)	C(1B)–C(7B)	1.490(6)	C(12B)–C(16B)	1.507(6)
		C(3A)–C(4A)	1.398(7)				

Table 6. Bond Angles (deg) for TMBZ

C(3)–C(2)–C(13)	119.3(4)	C(2A)–C(1A)–C(6A)	119.2(4)	C(2B)–C(1B)–C(6B)	119.3(4)
C(3)–C(2)–C(1)	119.8(4)	C(2A)–C(1A)–C(7A)	121.1(4)	C(2B)–C(1B)–C(7B)	119.9(4)
C(13)–C(2)–C(1)	120.9(4)	C(6A)–C(1A)–C(7A)	119.7(4)	C(6B)–C(1B)–C(7B)	120.7(3)
C(2)–C(3)–C(4)	121.0(4)	C(1A)–C(2A)–C(3A)	120.4(4)	C(1B)–C(2B)–C(3B)	120.1(4)
N(1)–C(4)–C(3)	119.8(4)	C(1A)–C(2A)–C(13A)	120.4(4)	C(1B)–C(2B)–C(13B)	121.3(4)
N(1)–C(4)–C(5)	121.3(4)	C(3A)–C(2A)–C(13A)	119.2(4)	C(3B)–C(2B)–C(13B)	118.6(4)
C(3)–C(4)–C(5)	118.9(4)	C(2A)–C(3A)–C(4A)	120.3(4)	C(2B)–C(3B)–C(4B)	120.5(4)
C(4)–C(5)–C(6)	121.3(4)	N(2A)–C(4A)–C(3A)	120.5(4)	N(1B)–C(4B)–C(3B)	120.7(4)
C(5)–C(6)–C(15)	119.0(4)	N(2A)–C(4A)–C(5A)	120.6(4)	N(1B)–C(4B)–C(5B)	120.4(4)
C(5)–C(6)–C(1)	119.4(4)	C(3A)–C(4A)–C(5A)	118.8(4)	C(3B)–C(4B)–C(5B)	118.9(4)
C(15)–C(6)–C(1)	121.6(4)	C(4A)–C(5A)–C(6A)	121.4(4)	C(4B)–C(5B)–C(6B)	121.4(4)
C(8)–C(7)–C(12)	118.7(4)	C(1A)–C(6A)–C(5A)	119.8(4)	C(1B)–C(6B)–C(5B)	119.8(4)
C(8)–C(7)–C(1)	121.1(4)	C(1A)–C(6A)–C(15A)	120.3(4)	C(1B)–C(6B)–C(15B)	120.6(4)
C(12)–C(7)–C(1)	120.2(4)	C(5A)–C(6A)–C(15A)	119.9(4)	C(5B)–C(6B)–C(15B)	119.6(4)
C(7)–C(8)–C(9)	119.8(4)	C(1A)–C(7A)–C(8A)	122.2(4)	C(1B)–C(7B)–C(8B)	122.1(4)
C(7)–C(8)–C(14)	120.9(4)	C(1A)–C(7A)–C(12A)	118.9(4)	C(1B)–C(7B)–C(12B)	118.9(3)
C(9)–C(8)–C(14)	119.3(4)	C(8A)–C(7A)–C(12A)	119.0(4)	C(8B)–C(7B)–C(12B)	119.0(4)
C(8)–C(9)–C(10)	121.5(4)	C(7A)–C(8A)–C(9A)	120.2(4)	C(7B)–C(8B)–C(9B)	119.8(4)
N(2)–C(10)–C(9)	119.9(4)	C(7A)–C(8A)–C(14A)	120.9(4)	C(7B)–C(8B)–C(14B)	120.8(4)
N(2)–C(10)–C(11)	121.3(4)	C(9A)–C(8A)–C(14A)	118.8(4)	C(9B)–C(8B)–C(14B)	119.4(3)
C(9)–C(10)–C(11)	118.8(4)	C(8A)–C(9A)–C(10A)	121.3(4)	C(8B)–C(9B)–C(10B)	121.6(4)
C(10)–C(11)–C(12)	120.8(4)	N(1A)–C(10A)–C(9A)	121.2(4)	N(2B)–C(10B)–C(9B)	120.3(4)
C(7)–C(12)–C(11)	120.3(4)	N(1A)–C(10A)–C(11A)	120.4(4)	N(2B)–C(10B)–C(11B)	120.9(4)
C(7)–C(12)–C(16)	120.9(4)	C(9A)–C(10A)–C(11A)	118.5(4)	C(9B)–C(10B)–C(11B)	118.7(4)
C(11)–C(12)–C(16)	118.8(4)	C(10A)–C(11A)–C(12A)	121.3(4)	C(10B)–C(11B)–C(12B)	120.5(4)
C(2)–C(1)–C(6)	119.5(4)	C(7A)–C(12A)–C(11A)	119.7(4)	C(7B)–C(12B)–C(11B)	120.2(4)
C(2)–C(1)–C(7)	120.4(4)	C(7A)–C(12A)–C(16A)	121.8(3)	C(7B)–C(12B)–C(16B)	120.1(4)
C(6)–C(1)–C(7)	120.0(4)	C(11A)–C(12A)–C(16A)	118.5(4)	C(11B)–C(12B)–C(16B)	119.7(4)

Table 7. Atomic Coordinates ($\times 10^4$) and Equivalent Isotropic Displacement Parameters ($Å^2 \times 10^3$) for DMBZ[a]

	x	y	z	U_{eq}
N(1)	3473(1)	−1890(2)	5548(1)	39(1)
N(2)	3597(1)	883(2)	953(1)	38(1)
C(1)	3695(1)	−620(2)	3603(1)	23(1)
C(2)	3884(1)	672(2)	4067(1)	26(1)
C(3)	3834(1)	200(2)	4702(1)	30(1)
C(4)	3584(1)	−1496(2)	4901(1)	28(1)
C(5)	3377(1)	−2764(2)	4443(1)	28(1)
C(6)	3439(1)	−2322(2)	3811(1)	26(1)
C(7)	3712(1)	−229(2)	2912(1)	23(1)
C(8)	2913(1)	−476(2)	2559(1)	28(1)
C(9)	2866(1)	−124(2)	1921(1)	31(1)
C(10)	3630(1)	534(2)	1608(1)	27(1)
C(11)	4439(1)	727(2)	1945(1)	27(1)
C(12)	4499(1)	341(2)	2587(1)	23(1)
C(13)	5424(1)	473(2)	2903(1)	33(1)
C(14)	4070(1)	2596(2)	3903(1)	37(1)

[a] U_{eq} is defined as one-third of the trace of the orthogonalized U_{ij} tensor.

Table 8. Bond Lengths (Å) and Angles (deg) for DMBZ[a]

N(1)–C(4)	1.406(2)	C(7)–C(12)	1.403(2)
N(2)–C(10)	1.410(2)	C(8)–C(9)	1.375(2)
C(1)–C(6)	1.401(2)	C(9)–C(10)	1.386(2)
C(1)–C(2)	1.406(2)	C(10)–C(11)	1.385(2)
C(1)–C(7)	1.489(2)	C(11)–C(12)	1.390(2)
C(2)–C(3)	1.389(2)	C(12)–C(13)	1.509(2)
C(2)–C(14)	1.509(2)	N(1)–H(2A)#1	2.34(2)
C(3)–C(4)	1.389(2)	N(2)–H(1B)#3	2.17(2)
C(4)–C(5)	1.391(2)	H(1B)–N(2)#4	2.17(2)
C(5)–C(6)	1.379(2)	H(2A)–N(1)#2	2.34(2)
C(7)–C(8)	1.397(2)		
C(6)–C(1)–C(2)	117.4(1)	C(8)–C(7)–C(12)	117.4(1)
C(6)–C(1)–C(7)	119.5(1)	C(8)–C(7)–C(1)	119.0(1)
C(2)–C(1)–C(7)	123.0(1)	C(12)–C(7)–C(1)	123.6(1)
C(3)–C(2)–C(1)	119.2(1)	C(9)–C(8)–C(7)	122.7(2)
C(3)–C(2)–C(14)	118.3(1)	C(8)–C(9)–C(10)	119.7(2)
C(1)–C(2)–C(14)	122.3(1)	C(11)–C(10)–C(9)	118.4(1)
C(4)–C(3)–C(2)	122.7(2)	C(11)–C(10)–N(2)	120.9(2)
C(3)–C(4)–C(5)	118.2(1)	C(9)–C(10)–N(2)	120.5(2)
C(3)–C(4)–N(1)	121.2(2)	C(10)–C(11)–C(12)	122.2(2)
C(5)–C(4)–N(1)	120.5(2)	C(11)–C(12)–C(7)	119.3(1)
C(6)–C(5)–C(4)	119.7(2)	C(11)–C(12)–C(13)	118.3(1)
C(5)–C(6)–C(1)	122.7(2)	C(7)–C(12)–C(13)	122.3(1)

[a] Symmetry transformations used to generate equivalent atoms: #1 = 0.5 − x, −y, 0.5 + z; #2 = 0.5 − x, −y, −0.5 + z; #3 = x, −0.5 − y, −0.5 + z; #4 = x, −0.5 − y, 0.5 + z.

Table 9. Torsion Angles (deg) for DMBZ

C(6)–C(1)–C(2)–C(3)	1.7(2)	C(4)–C(5)–C(6)–C(1)	−0.7(2)	C(8)–C(9)–C(10)–C(11)	3.4(2)
C(7)–C(1)–C(2)–C(3)	178.7(1)	C(2)–C(1)–C(6)–C(5)	−0.7(2)	C(8)–C(9)–C(10)–N(2)	179.3(2)
C(6)–C(1)–C(2)–C(14)	−173.5(1)	C(7)–C(1)–C(6)–C(5)	−177.8(1)	C(9)–C(10)–C(11)–C(12)	−2.2(2)
C(7)–C(1)–C(2)–C(14)	3.5(2)	C(6)–C(1)–C(7)–C(8)	57.1(2)	N(2)–C(10)–C(11)–C(12)	−178.0(2)
C(1)–C(2)–C(3)–C(4)	−1.5(2)	C(2)–C(1)–C(7)–C(8)	−119.8(2)	C(10)–C(11)–C(12)–C(7)	−1.4(2)
C(14)–C(2)–C(3)–C(4)	173.9(2)	C(6)–C(1)–C(7)–C(12)	−121.3(2)	C(10)–C(11)–C(12)–C(13)	175.9(1)
C(2)–C(3)–C(4)–C(5)	0.1(2)	C(2)–C(1)–C(7)–C(12)	61.8(2)	C(8)–C(7)–C(12)–C(11)	3.6(2)
C(2)–C(3)–C(4)–N(1)	−175.1(2)	C(12)–C(7)–C(8)–C(9)	−2.4(2)	C(1)–C(7)–C(12)–C(11)	−178.0(1)
C(3)–C(4)–C(5)–C(6)	1.0(2)	C(1)–C(7)–C(8)–C(9)	179.1(2)	C(8)–C(7)–C(12)–C(13)	−173.6(1)
N(1)–C(4)–C(5)–C(6)	176.2(1)	C(7)–C(8)–C(9)–C(10)	−1.1(2)	C(1)–C(7)–C(12)–C(13)	4.8(2)

Table 10. Atomic Coordinates (×10⁴) and Equivalent Isotropic Displacement Parameters (Å² × 10³) for BFBZ[a]

	x	y	z	U_{eq}		x	y	z	U_{eq}
N	3151(1)	4397(3)	5041(1)	29(1)	C(3)	4583(1)	2987(3)	5794(1)	23(1)
F(1)	6910(1)	2536(2)	6486(1)	39(1)	C(4)	3704(1)	4325(3)	5722(1)	22(1)
F(2)	6082(1)	−165(2)	5947(1)	43(1)	C(5)	3335(1)	5449(3)	6358(1)	26(1)
F(3)	6095(1)	93(2)	7154(1)	41(1)	C(6)	3842(1)	5260(3)	7042(1)	24(1)
C(1)	4728(1)	3951(3)	7126(1)	20(1)	C(7)	6026(1)	1325(3)	6522(1)	26(1)
C(2)	5090(1)	2800(3)	6484(1)	20(1)					

[a] U_{eq} is defined as one-third of the trace of the orthogonalized U_{ij} tensor.

Table 11. Bond Lengths (Å) and Angles (deg) for BFBZ[a]

N–C(4)	1.400(2)	F(3)–C(7)	1.331(2)	C(2)–C(3)	1.389(2)	H(1A)#1..N#2	2.496(1)
N–H(1A)	0.885	C(1)–C(6)	1.386(2)	C(2)–C(7)	1.487(2)	N#1..N#2[b]	3.374(2)
N–H(1B)	0.891	C(1)–C(2)	1.397(2)	C(3)–C(4)	1.386(2)	H(5A)#3..F(3)#1	2.493(2)
F(1)–C(7)	1.347(2)	C(1)–C(1)#1	1.497(3)	C(4)–C(5)	1.86(2)	C(5)#3..F(3)#1[b]	3.849(2)
F(2)–C(7)	1.340(2)			C(5)–C(6)	1.378(2)		

C(6)–C(1)–C(2)	117.2(1)	C(4)–C(3)–C(2)	120.8(2)	H(1A)–N–C(4)	112.6(1)	F(3)–C(7)–F(1)	105.5(1)
C(6)–C(1)–C(1)#1	118.9(2)	C(3)–C(4)–C(5)	118.5(1)	H(1B)–N–C(4)	113.89(9)	F(2)–C(7)–F(1)	105.1(1)
C(2)–C(1)–C(1)#1	123.9(2)	C(3)–C(4)–N	121.0(2)	C(6)–C(5)–C(4)	120.5(2)	F(3)–C(7)–C(2)	113.9(1)
C(3)–C(2)–C(1)	121.0(2)	C(5)–C(4)–N	120.4(2)	C(5)–C(6)–C(1)	122.1(2)	F(2)–C(7)–C(2)	112.8(1)
C(3)–C(2)–C(7)	118.0(1)	H(1A)–N–H(1B)	113.48	F(3)–C(7)–F(2)	106.2(1)	F(1)–C(7)–C(2)	112.6(1)
C(1)–C(2)–C(7)	121.1(1)						

[a] Symmetry transformations used to generate equivalent atoms: #1 = $-x+1, y, -z+3/2$; #2 = $1/2+x, 1/2+y, 3/2-z$; #3 = $x, -1+y, z$. [b] Not an interaction but noted for precision sake.

Table 12. Selected Torsion Angles (deg) for BFBZ[a]

C(6)–C(1)–C(1)#1–C(6)#1	−101.8(3)	C(1)–C(2)–C(3)–C(4)	0.0(2)	C(2)–C(1)–C(6)–C(5)	−0.4(2)
C(6)–C(1)–C(1)#1–C(2)#1	74.6(1)	C(7)–C(2)–C(3)–C(4)	179.7(2)	C(1)#1–C(1)–C(6)–C(5)	176.2(2)
C(2)–C(1)–C(1)#1–C(2)#1	−109.1(3)	C(2)–C(3)–C(4)–C(5)	−0.8(2)	C(3)–C(2)–C(7)–F(3)	−140.2(2)
C(6)–C(1)–C(2)–C(3)	0.6(2)	C(2)–C(3)–C(4)–N	−175.6(2)	C(1)–C(2)–C(7)–F(3)	39.5(2)
C(1)#1–C(1)–C(2)–C(3)	−175.9(1)	C(3)–C(4)–C(5)–C(6)	0.9(2)	C(3)–C(2)–C(7)–F(2)	−19.0(2)
C(6)–C(1)–C(2)–C(7)	−179.1(2)	N–C(4)–C(5)–C(6)	175.8(2)	C(1)–C(2)–C(7)–F(2)	160.6(1)
C(1)#1–C(1)–C(2)–C(7)	4.5(2)	C(4)–C(5)–C(6)–C(1)	−0.3(3)	C(3)–C(2)–C(7)–F(1)	99.7(2)
				C(1)–C(2)–C(7)–F(1)	−80.6(2)

[a] Symmetry transformations used to generate equivalent atoms: #1 = $-x+1, y, -z+3/2$.

Table 13. Viscosity and Solubility of Polyimides Derived from Substituted Benzidines

diamine	dianhydride[a]	$[\eta]$,[b] dL/g	solubility	diamine	dianhydride[a]	$[\eta]$,[b] dL/g	solubility
TMBZ	PMDA	insoluble	insoluble	DMBZ	HFDA	0.87	*m*-cresol, TCE
TMBZ	BTDA	1.6	*m*-cresol, TCE, NMP	DMBZ	DSDA	0.65	*m*-cresol, TCE
TMBZ	ODPA	1.4	*m*-cresol, TCE, NMP	DMBZ	BPDA	insoluble[c]	insoluble[c]
TMBZ	HFDA	1.6	*m*-cresol, TCE, NMP	BFBZ	PMDA	insoluble	insoluble
TMBZ	DSDA	1.3	*m*-cresol, TCE, NMP	BFBZ	BTDA	1.6[d]	*m*-cresol
TMBZ	BPDA	5.0	*m*-cresol, TCE	BFBZ	ODPA	1.1[d]	*m*-cresol, TCE,[e] NMP[f]
DMBZ	PMDA	insoluble	insoluble	BFBZ	HFDA	1.9[d]	*m*-cresol, TCE, NMP
DMBZ	BTDA	insoluble	insoluble	BFBZ	DSDA	1.0[d]	*m*-cresol, TCE
DMBZ	ODPA	insoluble	insoluble	BFBZ	BPDA	4.9[d]	*m*-cresol

[a] PMDA = pyromellitic dianhydride; BTDA = 3,3′,4,4′-benzophenonetetracarboxylic dianhydride; ODPA = 4,4′-oxydiphthalic anhydride; HFDA = 4,4′-(hexafluoroisopropylidene)diphthalic anhydride; DSDA = 3,3′,4,4′-diphenylsulfonetetracarboxylic dianhydride; BPDA = 3,3′,4,4′-biphenyltetracarboxylic dianhydride. [b] Intrinsic viscosities were measured in *m*-cresol at 30 °C. [c] The polyimide based on BPDA/DMBZ precipitated from *m*-cresol prematurely during the polymerization; however, the polymerization could be achieved in boiling *p*-chlorophenol (bp = 220 °C, mp = 43–45 °C) to yield polyimides with intrinsic viscosity $[\eta]$ = 10 dL/gm in *p*-chlorophenol at 60 °C (ref 20). [d] $[\eta]$ and solubility were taken from ref 17. [e] TCE = 1,1,2,2-tetrachloroethane. [f] NMP = *N*-methyl-2-pyrrolidinone.

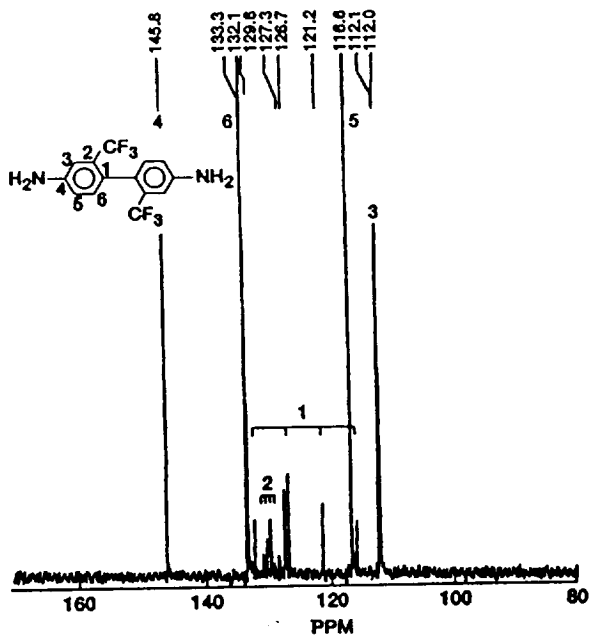

Figure 5. ^{13}C-NMR spectra of 2,2′-bis(trifluoromethyl)benzidine (BFBZ).

Table 14. ^{13}C Assignment for Substituted Benzidines

	DMBZ	TMBZ	BFBZ
C-1	130.70	130.58	127.34
C-2	137.25	137.16	129.94(q)
C-3	112.30	114.24	112.02
C-4	144.98	144.56	145.80
C-5	116.30	(114.24)	116.63
C-6	132.06	(137.16)	133.34
CH_3	19.88	19.90	
CF_3			123.95(q)

Table 15. Physical Properties of Polyimides Based on Substituted Benzidines

property	TMBZ–BPDA	DMBZ–BPDA	BFBZ–BPDA
T_g by TMA[a] (°C)	315	300	290
TGA/N_2 (5% wt loss, °C)	520	500	600
tensile modulus (GPA)[b]	75	150	130
tensile strength (GPa)[b]	2.0	3.5	3.2
elongation at break (%)[b]	2.7	4.0	4.0
density (g/cm^3)	1.37	1.40	1.45

[a] T_g was determined by thermal mechanical analysis (TMA) on a single fiber under different stresseses (σ), by extrapolation to σ = 0 as described in ref 11. [b] Data were obtained from ref 21.

as their ^{1}H-NMR for CH_3 substituents (δ = 1.82 for TMBZ and 1.97 for DMBZ in $CDCl_3$). The two CF_3 groups in BFBZ are on the opposite side of the x–z plane (anti) containing two amino nitrogens as predicted in terms of the lower energy state by reported molecular modeling;[9,10] however, the two CH_3 groups in DMBZ are unexpectedly located on the same side of the x–z plane (syn), although the two phenyl rings are twisted out of the plane. The torsional angles measured by X-ray crystallography for DMBZ and BFBZ (ϕ = 75° and 59°, respectively) are in contrast to the dihedral angles predicted by previous molecular modeling, which indicated that the lowest energy conformations were achieved in noncoplanar biphenyl derivatives when the dihedral angles of two phenyl rings were close to 90° or 270°.[9,10,21] More surprisingly, all the molecular modelings have failed to anticipate that the two CH_3 groups in DMBZ would be located on the same side (syn) of the x–z plane. All the modeling inherently places the substituents at the 2,2′-position on the opposite (anti) to yield the lower energy conformation. One might explain after the fact that the reason that two CF_3 substituents would occupy the opposite sides (anti) on two phenyl rings is due to the balance of dipole moments on BFBZ, which lowers the potential energy as well as steric hindrance due to the slightly larger size of the F atom relative to the H atom. Additionally, the C–F bond length in BFBZ is 1.3 Å, relative to the C–H bond length of 1.1 Å in DMBZ. However, the fact that two CH_3 groups occupied the same side (syn) is still beyond expectation.

Table 1[illegible] indicates that TMBZ-based polyimides are generally more soluble than DMBZ and BFBZ containing polyimdes in organic solvents, such as NMP, *m*-cresol, or 1,1,2,2-tetrachloroethane. This phenomenon might be explained in terms of the greater free volume between TMBZ–BPDA polymer chains relative to BFBZ–BPDA and DMBZ–BPDA. The larger torsional angle and the four CH_3 on both sides of the x–z plane in TMBZ inevitably would occupy a bigger volume, relative to the two CH_3 on the adjacent side of DMBZ. The unit cell data (V = 4149.2 Å^3 per 13 formula units for TMBZ, V = 2311.4 Å^3 per 8 formula units for DMBZ, V = 1334.95 Å^3 per 4 formula units for BFBZ) show that the volume per formula unit decreases in the order of TMBZ > BFBZ > DMBZ. However, the real proof of actual free volume for these polyimdes would require the X-ray single crystal structures of the corresponding polymers. Furthermore, the improved solubility of BFBZ–BPDA over DMBZ–BPDA also is attributed to the enhanced organosolubility of CF_3 group over CH_3, since the torsional angle between the two phenyl rings on BFBZ is smaller than that of DMBZ. The small torsional angle in BFBZ (ϕ = 59°) *versus* ϕ = 75° in DMBZ reflects the fact that the two CF_3 substituents were far apart from each other, relative to the two CH_3 groups located adjacent to each other with significant steric hindrance.

As shown in Table 15, the glass transition temperatures (T_g) of polyimides derived from substituted benzidines and BPDA decrease in the order of

TMBZ–BPDA > DMBZ–BPDA > BFBZ–BPDA

The steric hindrance of the four methyl substituents on the two phenyl rings of TMBZ apparently contribute to a higher rotational barrier to the polymer chains during the glass transition state, relative to that of the 2,2′-substituted DMBZ and BFBZ. Furthermore, the two adjacent methyl groups on DMBZ certainly create a higher rotational barrier than that of the two CF_3 groups that were far apart. The thermal gravimetric analysis (TGA) indicated that the CF_3 substituent exhibited higher thermo-oxidative stability than CH_3. The better tensile properties of DMBZ–BPDA over TMBZ–BPDA and BFBZ–BPDA are in part due to the fact that DMBZ–BPDA had highest molecular weight, resulting from the polymerization in higher boiling *p*-chlorophenol. The reported intrinsic viscosities are for DMBZ–BPDA [η] = 10 dL/g in *p*-chlorophenol[20] at 60 °C *versus* [η] = 5.0 dL/g for TMBZ–BPDA and [η] = 4.9 dL/g for BFBZ–BPDA in *m*-cresol at 30 °C. Additionally, the electron-donating CH_3 groups on DMBZ could increase the nucleophilicity of DMBZ relative to the electron-withdrawing CF_3 in BFBZ, thus resulting in the higher molecular weight and higher viscosity for DMBZ–BPDA polyimide. Moreover, the slower crystallization rate which promotes higher crystal orientation and draw ratio, as displayed by DMBZ–BPDA during

the drawing process, could also contribute to its higher tensile properties.[22,23] However, BFBZ–BPDA exhibits higher degradation temperature (T_d = 600 °C) than either TMBZ–BPDA or DMBZ–BPDA (Table 15), because CF_3 substituents are thermally more stable than CH_3.

Summary and Conclusions

Polyimides prepared from 2,2′,6,6′-tetrasubstituted 4,4′-biphenyldiamine exhibit enhanced solubility relative to 2,2′-disubstituted benzidine, due to the larger torsional angle between two phenyl rings as revealed by X-ray crystallography (ϕ = 83° for TMBZ, ϕ = 75° for DMBZ, and ϕ = 59° for BFBZ). Unexpectedly, the two CH_3 groups on DMBZ were located on the same side (syn) of the $x-z$ plane in an adjacent location whereas the two CF_3 substituents on BFBZ were far apart on the opposite side (anti) of the $x-z$ plane. Furthermore, the CF_3 substituents impart not only better thermooxidative stability but also increased solubility in the resulting polyimides, relative to CH_3 groups.

Acknowledgment. The authors thank Dr. Makoto Kaji of Hitachi, Japan, for providing a small quantity of 2,2′-dimethylbenzidine for X-ray crystallography.

Supporting Information Available: Tables of H atom coordinates and isotropic displacements for 2,2′,6,6′-tetramethylbenzidine (TMBZ), for 2,2′-dimethylbenzidine (DMBZ), and for 2,2′-bis(trifluoromethyl)benzidine (BFBZ) (9 pages); observed and calculated structure factors for TMBZ, DMBZ, and BFBZ (21 pages). Ordering information is given on any current masthead page.

References and Notes

(1) Blair, T. I.; Morgan, P. M.; Killian, F. L. *Macromolecules* **1977**, *10* (6), 1396.
(2) Percha, Im J.; Yeakle, D. S. *Mater. Res. Soc. Symp. Proc. (Mater. Sci. Eng. Rigid-Rod Polym.)* **1989**, *234*, 307.
(3) Navarro, F. *Macromolecules* **1991**, *24*, 6622.
(4) Morgan, P. M. *Macromolecules* **1977**, *10* (6), 1381.
(5) Becker, K. H.; Schmidt, H-W. *Macromolecules* **1992**, *25*, 6784.
(6) Bhowmik, P. K.; Atkin, E. D. T.; Lenz, R. W. *Macromolecules* **1993**, *26*, 440.
(7) Schmidt, H.-W.; Guo D. *Makmol. Chem.* **1988**, *189*, 2029.
(8) Rogers, H. G.; Gaudiana, R. A.; Hollinsed, W. C.; Kalyanaraman, P. S.; Manello, J. S.; McGrown, C.; Minns, R. A.; Sahatjian, R. *Macromolecules* **1985**, *18*, 1058.
(9) Tsuzuki, S.; Tanabe, K.; Nagawa, Y.; Nakanishi, H. *J. Mol. Struct.* **1988**, *178*, 277.
(10) Coburn, J. C.; Soper, P. D.; Auman, B. C. *Macromolecules* **1995**, *28*, 3253.
(11) Wu, T. M.; Chvalun S.; Blackwell, J.; Cheng, S. Z. D.; Wu, Z.; Harris, F. W. *Polymer* **1995**, *36* (11), 2123.
(12) Eashoo, Mark; Shen, D.; Wu, Z.; Lee, C. J.; Harris, F. W.; Cheng, S. Z. D. *Polymer* **1993**, *15*, 3209.
(13) Cheng, S. Z. D.; Lee, S. K.; Barley, J. S.; Hsu, S. L. C.; Harris, F. W. *Macromolecules* **1991**, *24*, 1883.
(14) Cheng, S. Z. D.; Arnold, F. E.; Zhang, A.; Hsu, S. L. C.; Harris, F. W. *Macromolecules* **1991**, *24*, 5856.
(15) Matsuura, T.; Hasuda, Y.; Nishi, S.; Yamada, N. *Macromolecules* **1991**, *24*, 5001.
(16) Chuang, K. C.; Vannucci, R. D.; Ansari, I.; Cerny, L. L.; Scheiman, D. A. *J. Polym. Sci. Chem. Ed.* **1994**, *32*, 1341.
(17) Chuang, K. C. *High Perform. Polym.* **1995**, *7*, 81.
(18) Harris, F. W.; Hsu, S. L. C.; Tso, C. C. *Polym. Prepr.* **1991**, *32* (2), 97.
(19) Cheng, S. Z. D.; Wu Z.; Eashoo, M.; Hsu, S. L. C.; Harris, F. W. *Polymer* **1991**, *32* (10), 1803.
(20) Eashoo, M.; Wu, Z.; Zang, A.; Shen, D.; Tse, C.; Harris, F. W.; Cheng, S. Z. D. *Macomol. Chem. Phys.* **1994**, *195*, 2207.
(21) Arnold, F. E., Jr.; Bruno, K. R.; Shen, D.; Eashoo, M.; Harris F. W.; Cheng, S. Z. D. *Polym. Eng. Sci.* **1996**, *33* (21), 1373.
(22) Cheng, S. Z. D.; Wu, Z.; Hull, D. L.; Chuang, K. C. *HITemp Rev. 1995, NASA CP 10178*, vol. 1, Article 6.
(23) Wu, Z.; Zhang, A.; Shen, D.; Leland, M.; Harris, F. W.; Cheng, S. Z. D. *J. Thermal. Anal.* **1996**, *46* (3-4), 719.
(24) Copyright 1989, 1990, Siemens Analytical X-Ray Instruments, Inc., Madison, WI.
(25) Sheldrick, G. M. *SHELXL-93 Program for the refinement of crystal structures*. University of Gottingen, Germany, 1993.
(26) An extinction parameter, x, is defined where F_c is multiplied by $k[1 + 0.001 \times F_c^2\lambda^3/\sin(2\theta)]^{-1/4}$ with k = overall scale factor.
(27) $wR2 = [\Sigma[w(F_o^2 - F_c^2)^2]/\Sigma[w(F_o^2)^2]]^{1/2}$. Weighted R-factors are based on F^2 and are statistically about twice as large as those based on F.
(28) $R1 = \Sigma||F_o| - |F_d||/\Sigma|F_o|$. Conventional R-factors are calculated using the observed criterion. This criterion is irrelevant to the choice of reflections used in the refinement.
(29) $S = [\Sigma[w(F_o^2 - F_c^2)^2]/(n - p)]^{1/2}$. The goodness-of-fit is based on F^2 where n = number of data and p = number of parameters refined.

MA970309B